

MINERALOGY, PETROLOGY AND GEOCHEMISTRY OF AMPHIBOLITES FROM THE KALNIK MT. (SAVA UNIT, NORTH CROATIA): IMPLICATIONS FOR THE EVOLUTION OF NORTH-WESTERNMOST PART OF THE DINARIC-VARDAR BRANCH OF MESOZOIC TETHYS

Branimir Šegvić^{*,✉}, †Boško Lugović^{**}, Damir Slovenec^{***} and Hans-Peter Meyer[°]

* Department of Earth Sciences, University of Geneva, Switzerland.

** Faculty of Mining, Geology and Petroleum Engineering, University of Zagreb, Croatia.

*** Croatian Geological Survey, Zagreb, Croatia.

° Institute for Geosciences, Ruprecht-Karls-Universität Heidelberg, Germany.

✉ Corresponding author: email: branimir.segvic@unige.ch

Keywords: amphibolite, ophiolites, metamorphic sole, Sava Unit, Neotethys. Kalnik Mt., Dinarides, North Croatia.

ABSTRACT

This paper brings a first comprehensive set of mineralogical, petrological and geochemical data of amphibolites associated with mantle peridotites in the Upper Jurassic to mid Lower Cretaceous ophiolite mélange of Kalnik Mt. in northern Croatia. This mélange is emplaced in a Paleogene sedimentary succession. Metamorphic evolution of the amphibolites and the nature of their igneous protoliths are discussed in the frame of late history development of north-western branch of Dinaric-Vardar Tethys. Primary amphibolite assemblages consist of pargasite-magnesio-hornblende and oligoclase-bytownite (*common amphibolite*) + almandine-grossular-rich garnet (*garnet amphibolites*) + clinopyroxene (*clinopyroxene amphibolites*). Minimum equilibration temperature for the amphibole-plagioclase pairs was estimated at $660\pm 40^\circ\text{C}$, whereas the peak conditions ($790\pm 20^\circ\text{C}$ at 0.79 to 1.04 GPa) were recorded in garnet amphibolite. Retrograde parageneses (albite, actinolite, clinozoisite, titanite, chlorite, pumpellyite, and 'metamorphic vermiculite') correspond to greenschist to sub-greenschist facies conditions. Protolith REE patterns match modern ocean ridge basalts ($\text{La}_N/\text{Lu}_N = 0.51\text{-}0.82$) whilst the normalized multi-element diagram shows slight negative HFSE anomalies ($\text{Nb}_N/\text{La}_N = 0.44\text{-}0.90$), diagnostic for a subduction-zone geochemical signature. Overall, geochemical data suggest back-arc basin (BAB) tholeiitic mafic extrusives (lack of Eu anomaly) and IAT-like cumulates (Eu positive anomaly) as amphibolite precursors. The Kalnik Mt. amphibolites are proposed to have formed during the incipient intraoceanic subduction following the model of metamorphic sole at the expense of an oceanic crust originated at the ridge of a back-arc marginal basin. The metamorphism must have taken place during Tithonian (?) as inferred from the protolith age. According to the geological evidences the back-arc magmatic regime was active until the final closure of Mesozoic Tethys in Cretaceous by the obduction of Dinaric ophiolites onto the NW margins of Adria microplate, when part of the metamorphic sole must have been exhumed and obducted together with the rest of ophiolite sequence.

INTRODUCTION

Within main ophiolitic belts of the Dinarides, Albanides and Hellenides, the occurrences of metamorphic rocks of the Jurassic age are well documented (e.g., Gjata et al., 1992; Dilek and Whitney, 1997; Bébien et al., 2000; Fig. 1). In the neighbouring Western Vardar ophiolites in the sense of Schmid et al. (2008; Fig. 1), or more precisely in the Zagorje-Mid-Transdanubian Zone (ZMTDZ; Pamić and Tomljenović, 1998) or Sava Unit (Schmid et al., 2008; Haas et al., 2000; Fig. 2), where the remnants of the Triassic and Jurassic Neotethys are both reported (Lugović et al., 2007; 2015; Slovenec et al., 2011), the outcrops of high-grade metamorphic rocks have not yet been reported (e.g., Slovenec and Pamić, 2002; Lugović et al., 2007).

Looking back in the geological records the history of the Sava Unit is quite complex. The Paleotethys back-arc oceans known in the literature as Meliata-Maliac or Meliata-Hallstatt (e.g., Stampfli et al., 2002) experienced constant shortening during the Jurassic period owing to the rotation of Africa with respect to Europe (Cavazza et al., 2004; Burke, 2011). This eventually led to the opening of the Vardar supra-subduction ocean during the roll-back of the Meliata-Maliac. An ensuing middle to Late Jurassic intraoceanic convergence of Western Vardar realm was manifested in the area of the Sava Unit by the subduction of an active oceanic ridge, developed arc activity, and related local extensions with occurrences of back-arc magmatism (Slovenec and Lu-

gović, 2009; Bortolotti et al., 2013). The final closure of Neotethys is inferred to correspond to the Barremian-Aptian, constrained in the Sava Unit by the age of greenschists of the Mt. Medvednica (Belak et al., 1995) that were thrust onto the Adria continental margins (Lugović et al., 2006).

Only recently the occurrence of amphibolites associated to altered ultramafic rocks was reported within the ophiolitic mélange of Kalnik Mt. (Fig. 3; Šegvić et al., 2005). Understanding the original geological setting of amphibolites was, however, difficult since the southern portion of the Sava Unit lacks any real ophiolitic complexes, and ophiolitic rocks are rather exposed in several separate ophiolite mélange sectors (e.g., Haas et al., 2000; Slovenec and Lugović, 2012). Moreover, the various blocks of magmatic and sedimentary rocks enclosed in the matrix of ophiolite mélange are frequently juxtaposed and vary both in age and lithology (e.g., Halamić, 1988; Slovenec and Pamić, 2002). An earlier radiometric dating of amphibolites yielded an age of 118 ± 8 Ma (Šegvić et al., 2005) but due to the uncertainties of K-Ar dating of amphiboles exposed to low-grade conditions (e.g., Jappy et al., 2001) it is highly plausible that such an obtained age may not represent the true age of metamorphism. Despite the complex geology of Sava Unit, the intimate proximity of amphibolites and overlying peridotites may be the sign of their common tectono-metamorphic history, possibly through the model of metamorphic sole, which in the rest of the Dinaride Ophiolite Zone (after Lanphere et al., 1975) gave rise to the formation of numerous

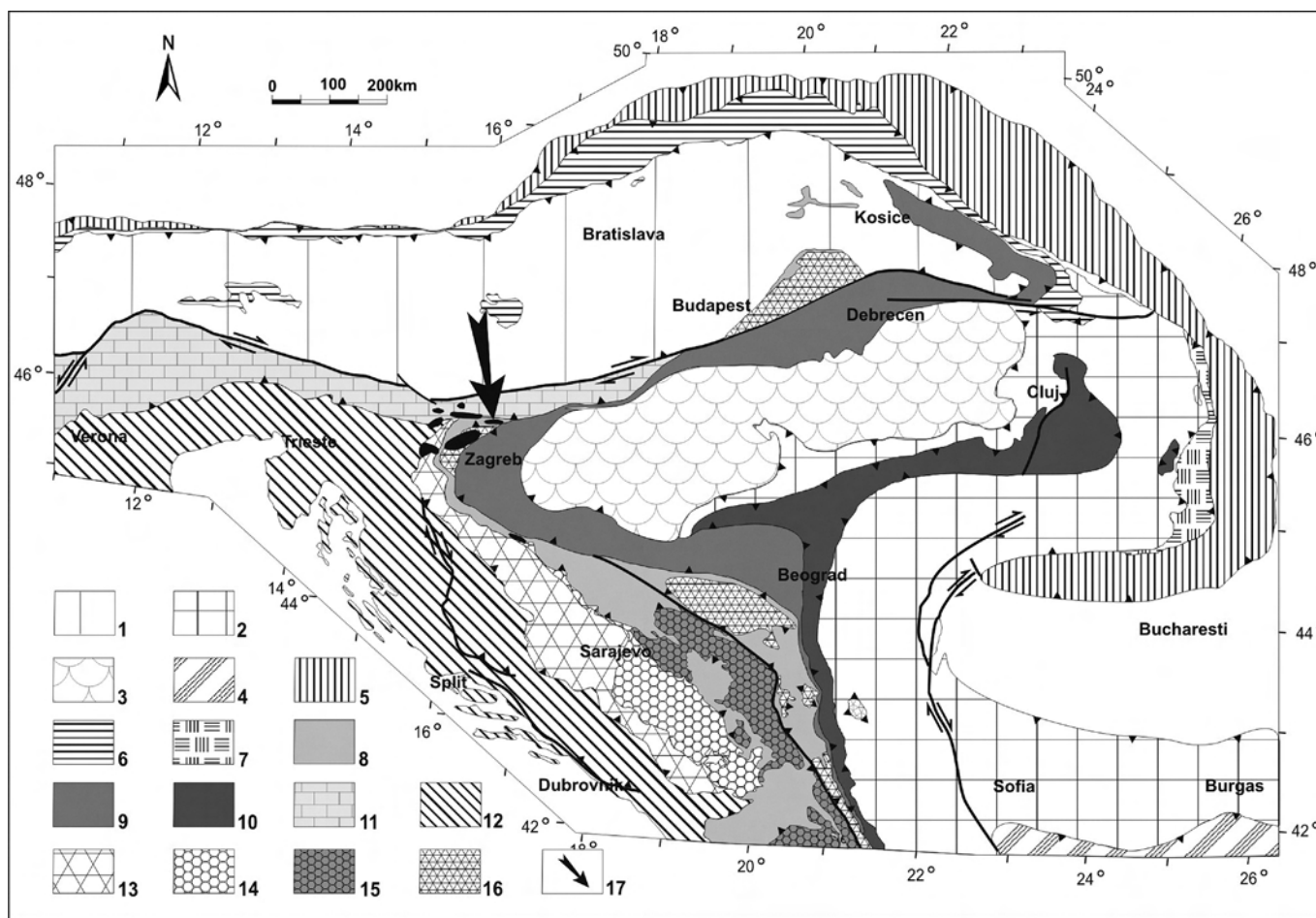


Fig. 1 - Geotectonic sketch map of the major tectonic units of the Alps, Carpathians and Dinarides (simplified after Schmid et al., 2008). Legend: 1- Adria derived far-travelled nappes Alps and W. Carpathians: ALCAPA (L. Austrialpine and Taticum, northern and southern margin of Meliata, Eoalpine high-pressure belt); 2- Europe-derived units: Dacia (Central Balkan and Prebalkan, Danubian, Helvetic, Subpenninic, Infrabucovinian, Getic, Sredna Gora, Serbo-Macedonian, Supragetic, Subbucovinian, Bucovinian, Biharia); 3- mixed European and Adriatic affinities: Tisza (Mecsek, Bihar, Codru); 4- inner Balkanides (Rhodope, Strandja); 5- Miocene thrust belt (thrust internal foredeep, Marginal Folds, Tarcau, Skole, Audia, Macia, Convolute Flysch, Subsilesian, Silesian, Dacia); 6- Ophiolites oceanic accretionary prisms: 6- Valais, Rhenodanubian, Magura, Pieniny, Klippen belt; 7- Ceahlau-Severin; 8- Meliata, Darnó-Szarvaskő, Dinaric, Western Vardar, Mirdita; 9- Piemont-Liguria, Vahicum, Inacovce-Krisevo, Szolnok, Sava; 10- Transylvanian, South Apuseni, Eastern Vardar; 11- Southern Alps; 12- Adriatic Plate, High Karst and Dalmatian Zone; 13- Pre-Karst and Bosnian Flysch; 14- East Bosnian-Durmitor; 15- Drina-Ivanjica, Korab, Pelagonides; 16- Bükk, Jadar, Kopaonik; 17- black arrow indicates the Kalnik Mt. investigated area.

amphibolite and granulite occurrences resulting from the Late Jurassic Neotethyan contraction (e.g., Operta et al., 2003). Alternatively, the Kalnik Mt. amphibolites stand for a product of regional metamorphism - an event that caused the formation of greenschists of the Mt. Medvednica during the Neotethyan obduction - which would make the analysed amphibolites contemporaneous to the ophiolite emplacement in the Early Cretaceous.

It is the aim of this paper to thoroughly report on the overall mineralogical, petrological and geochemical characteristics of amphibolites reported from the ophiolite mélangé of the Kalnik Mt. in order to shed more light on their metamorphic history and character of original (igneous) protolith. In addition, the correlation of the geochemical and petrological characteristics of studied rocks with the suites of various magmatic rocks cropping out within the broader Sava Unit of NW Dinarides, served as a basis to discuss a geotectonic affinity of suggested protoliths and plausible geodynamic scenarios which might have governed the formation of amphibolites recovered at the Kalnik Mt. in NW Croatia.

GEOLOGICAL SETTING

The Kalnik Mt. is an intra-Pannonian "inselberg" situated in the Sava Unit (after Haas et al., 2000; Fig. 2) or ZMTZD after Pamić and Tomljenović (1998). The Sava Unit is about 100 km wide and approximately 200 km long sheared belt sandwiched between the two regional fault systems: the Zagreb-Zemplin (ZZL) and the Periadriatic lineament (PL). The ZZL confines the Sava Unit south-westward towards Tisza Mega-unit, whilst the PL defines the northern border of Sava Unit to Austroalpine units and Pelso Unit (Fig. 2). Although the Sava Unit, i.e. ZMTZD, consists of mixed Dinaric and South Alpine tectonostratigraphic units (e.g., Haas et al., 2000), its affiliation to the Dinarides and their ophiolites is largely accepted (Pamić and Tomljenović, 1998). The Kalnik Mt. region consists of sedimentary rocks of different age associated with ophiolites (Pamić, 1997a; Fig. 3a-b). These include up to a few decametres to kilometre large fragments and blocks of oceanic provenance, such as tholeiitic basalts with dolerites and gabbros along with sporadic occurrences of mafic and ultramafic cumulates.

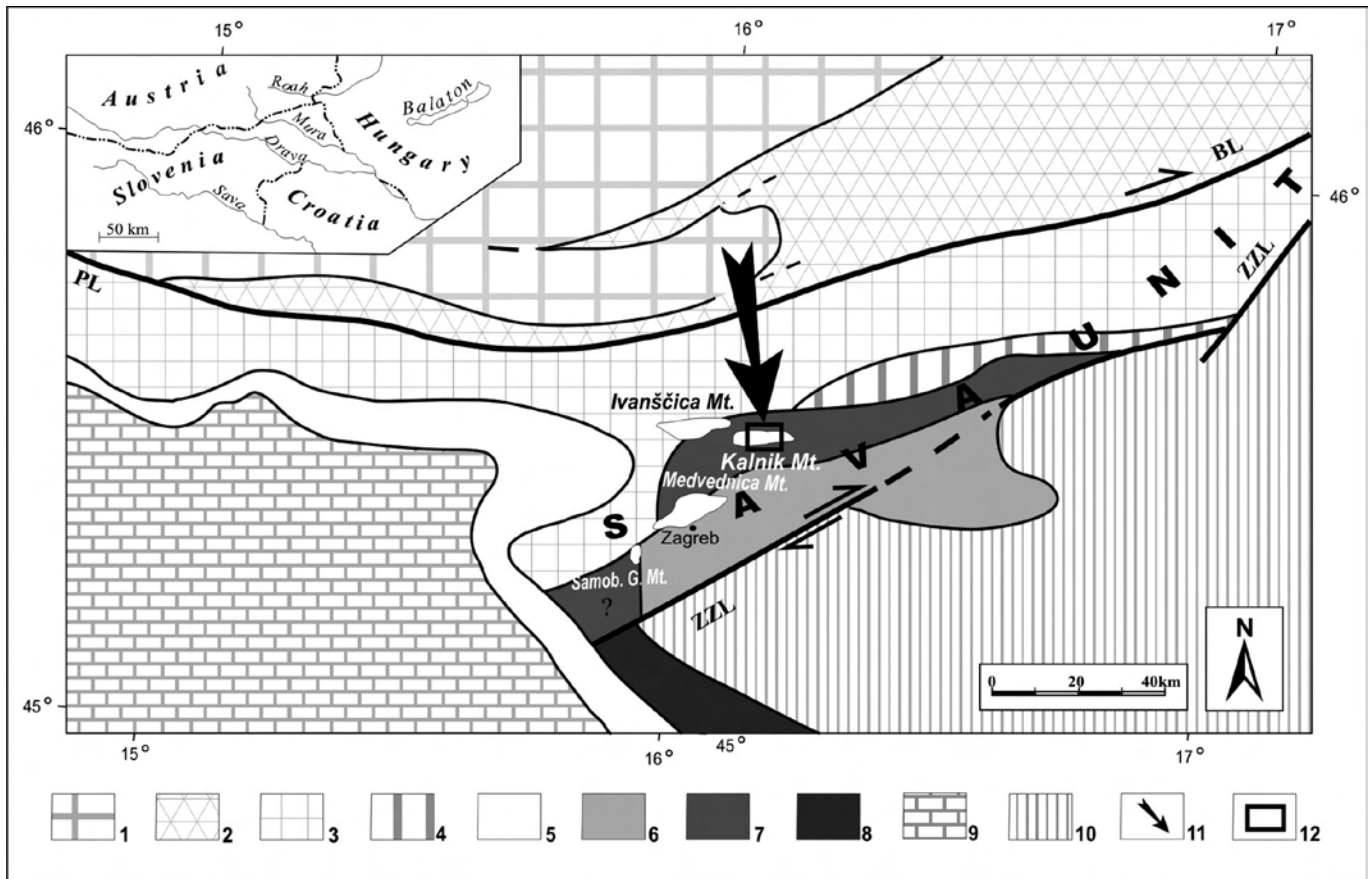


Fig. 2 - Sketch map of the structural units and major lineaments (modified after Haas et al., 2000). Insert map: geographic setting of the area presented in the sketch map. Legend: 1- Austroalpine units; 2- Pelso Unit; 3- South Alpine units and Julian-Savinja and South Karawanken units; 4- South Zala Unit; 5- Central Slovenian and Bosnian units; 6- Medvednica Unit; 7- Kalnik Unit; 8- Internal Dinaridic Unit (Vardar Unit); 9- External Dinaridic Unit; 10- Tisza Mega-Unit; 11- black arrow indicates the Kalnik Mt. study area; 12- box indicates the area shown on the Figure 3a; BL- Balaton Lineament; ZZZL- Zagreb-Zemplin Lineament; PL- Periadriatic Lineament.

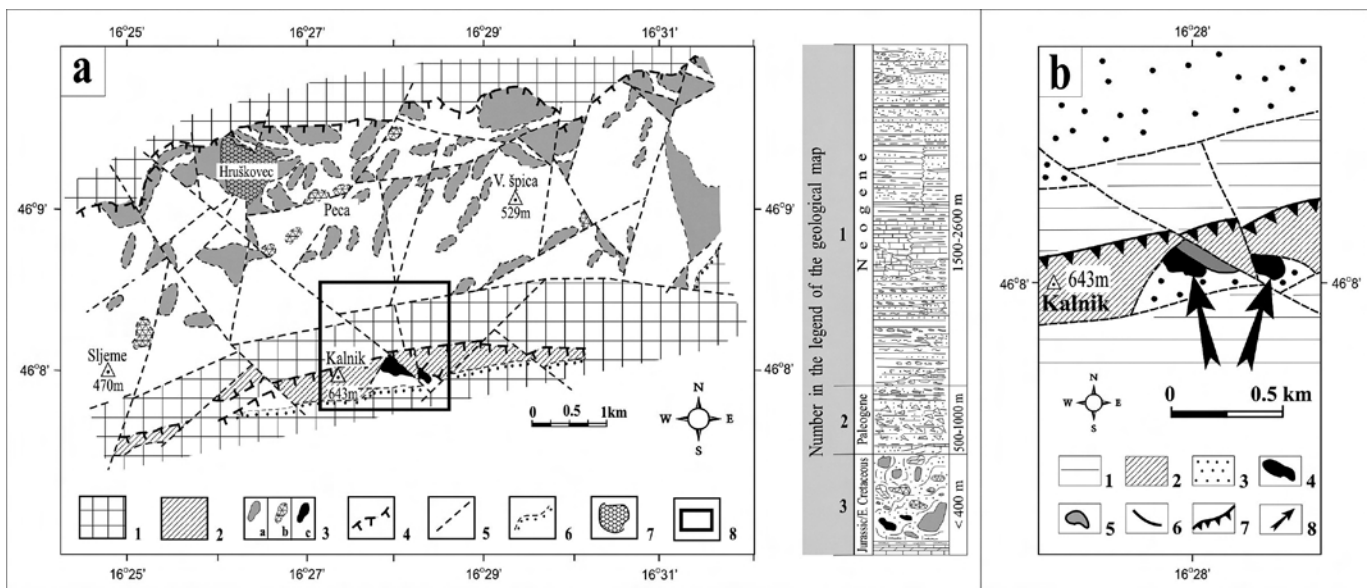


Fig. 3 - (a) Simplified geological map and stratigraphic column of Kalnik Mt. (modified after Šimunić et al., 1982 and Halamić 1999). Legend: 1- Neogene sedimentary rocks; 2- Paleogene sedimentary rocks; 3- Jurassic/Early Cretaceous ophiolite mélangé with blocks of: 3a- basalt, 3b- gabbro, 3c- amphibolite, tectonite peridotite and Triassic-Jurassic radiolarites, sandstones and shales (not separated on the maps); 4- reverse or thrust faults; 5- normal faults; 6- discordance line, tectonic-erosion discordance; 7- quarry; 8- detail shown on the geological sketch map 3b. (b) Sketch map of the investigated locations (modified after Šimunić et al., 1982). Legend: 1- Neogene sedimentary rocks; 2- Paleogene sedimentary rocks; 3- Ophiolite mélangé; Blocks in ophiolite mélangé: 4- amphibolites; 5- tectonite peridotite; 6- normal faults; 7- thrusts; 8- sample location.

The entire association shows a “block-in-matrix” fabric, typical for chaotic ophiolitic complexes, and it is referred to as a dismembered ophiolitic *mélange* (Lugović et al., 2007; Slovenec et al., 2011; Fig. 3a-b). This *mélange*, called the Kalnik Unit (after Haas et al., 2000; Fig. 2), comprises ophiolitic suites, mostly consisting of extrusive rocks and pillow basalts associated with radiolarian cherts that characterize all of the major inselbergs of NW Croatia (Mountains of Kalnik, Ivanščica, Samoborska Gora and Medvednica; Fig. 2; Slovenec and Lugović, 2009; Slovenec et al., 2010; 2011), whereas the *mélange* from the Medvednica Mt. also contains gabbroic rocks (Slovenec and Lugović, 2008). Owing to the lithological peculiarities, the part of the Sava Unit comprising the Kalnik Mt. and the neighbouring inselbergs is often considered as a corner oceanic branch that spatially “connects” Vardar-Dinaric ophiolites located to the southwest and Meliata-Maliac ophiolites to the northeast (e.g., Slovenec et al., 2011). Palynomorph assemblages from the *mélange* sedimentary matrix confined the accretion age of the Kalnik Mt. ophiolites to the Middle Jurassic to Early Cretaceous time (Babić et al., 2002). After the accretion, these rocks underwent the emplacement onto the eastern continental margins of the Adria Plate during the Aptian to Palaeocene timespan (Pamić and Tomljenović, 1998; Pamić, 2002). There are arguments suggesting that Sava Unit was displaced by the translation and rotation along the ZZL in NE direction, finally reaching its present position during the Middle Miocene (Pamić, 1997a; Tomljenović et al., 2008; Fig. 2).

Surface geology of the Kalnik Mt. comprises Neogene clastic sedimentary rocks along with the portions of heterogeneous ophiolitic *mélange* (Fig. 3a-b). In the *mélange*, the ophiolitic blocks are dominantly encountered, whereas the olistoliths of sedimentary origin (i.e., greywacke, minor shale, cherts, and scarce Triassic limestones) and the non-ophiolite suites of alkali basalts are only sporadically reported (e.g., Šimunić et al., 1982; Slovenec et al., 2011; Fig. 3a). The associated radiolarian cherts constrain the age of igneous rock fragments to the period of the Middle Triassic to Late Jurassic (Slovenec et al., 2011 and references therein). Ophiolite *mélange* is mainly in tectonic contact with the youngest Neogene and Pleistocene sedimentary rocks and the Kalnik Mt. central ridge consists of Paleogene carbonate breccias thrust over Neogene sedimentary rocks (Šimunić et al., 1982; Fig. 3a-b). Only in the Kalnik Mt. central ridge, Neogene sedimentary rocks transgressive overlap the ophiolite *mélange*. *Mélange* is dominantly composed of mafic extrusives, showing various geochemical affinities consistent with their distinct geotectonic formation setting in a period from the Illyrian to the late Oxfordian (Slovenec et al., 2011). Jurassic gabbros are also reported from the Kalnik Mt. ophiolitic *mélange*, occurring as hectometre-sized homogenous blocks (e.g., Vrkljan and Garašić, 2004; Lugović et al., 2015). However, some gabbroic blocks that appear as fault-bounded tectonic inclusions subsequently embedded in the *mélange* during ophiolite emplacement have been proved to present evidence of Cretaceous magmatism in the back-arc ridge setting (Lugović et al. 2015). Moreover several tectonic slices of mantle peridotites were exhumed along the mountain ridge tectonic zone (Šimunić et al., 1981). One of them is a few hundred meters large composite slice composed of serpentinized lherzolites (Lugović et al., 2007), which is underlain by ortho-amphibolites (Šegvić et al., 2005; Fig. 3b). Both rock types, amphibolites and serpentinites appearing in a small area of exposure, show characteristic foliation and banding, which may suggest a common

tectonic-metamorphic history. Amphibolites occur in the form of hectometre-sized blocks placed within the ophiolitic *mélange* that is found tectonically inserted in the Palaeogene sedimentary succession (Šimunić et al., 1982).

ANALYTICAL METHODS

Chemical composition of mineral phases from 8 thin-sections was measured by electron probe microanalyzer (EPMA) at the Institute of Geosciences (University of Heidelberg/Germany), using CAMECA SX51, equipped with five wavelength-dispersive spectrometers. Operating parameters include 15 kV accelerating voltage, 20 nA beam current, ~ 1 μm beam size, and 10 seconds counting time for all elements. Natural minerals, oxides (corundum, spinel, hematite, and rutile), and silicates (albite, orthoclase, anorthite, and wollastonite) were used for calibration. The measurements relative error was less than 1%. Raw data were corrected for matrix effects using the PAP algorithm (Pouchou and Pichoir, 1984; 1985) implemented by CAMECA. Mineral phase formula calculations were done using a software package designed by H-P. Meyer (University of Heidelberg/Germany).

Bulk-rock powders for chemical analyses of 8 amphibolite samples were obtained from rock chips free of veins. The samples were analysed for major and trace elements by ICP-MS at Actlab Laboratories (Ancaster/Canada). International mafic rocks were used as standards. Loss on ignition (LOI) was acquired by weight difference, after ignition at 1000°C for 1 hour. Major element and trace element concentrations were measured with an accuracy not exceeding 1% and 5%, respectively.

Automated mineral and textural characterization was performed using a FEI QEMSCAN[®] Quanta 650F facility at the Department of Earth Sciences (University of Geneva/Switzerland). This technique is based on automated scanning electron microscopy (SEM) coupled with EDS unit. Mineral phase identification relies on the combination of back-scattered electron (BSE) brightness values, low-count energy-dispersive X-ray spectra (EDS) and X-ray count rate giving information on the elemental composition (Gottlieb et al., 2000). Following the acquisition, individual X-ray spectrum is compared against a library of known spectra and a mineral name is assigned to each individual acquisition point. The X-ray EDS spectra library is provided by FEI Company and has been further developed in-house using different natural standards. Measurements were performed on the carbon-coated samples at high vacuum conditions using an acceleration voltage of 25 kV and probe current of 10 nA. The X-ray acquisition time was 10 ms per pixel with a point-spacing of 2.5 μm . Up to 122 individual fields were measured in each sample whereby the size of single field was 1.5 x 1.5 mm. Carbon-coated thin sections were used for SEM-EDS investigations. Crystal morphology, shapes, and mineral associations were studied by high-magnification back-scattered electron (BSE) and secondary electron (SE) imaging using QEMSCAN[®] facility operated in SEM mode under high vacuum. A variety of acceleration voltages and beam size conditions were employed to assure the best imaging conditions.

Geothermometric calculations are based on the compositions of thermodynamically equilibrated pairs of amphibole and plagioclase (Holland and Blundy, 1994). Metamorphic pressures are estimated using the geobarometer of Kohn and

Spear (1990) calibrated on the basis of equilibrium of coexisting amphibole, garnet, and plagioclase. All the results of geothermobarometric calculations are provided in Table 6. Due to complete retrogression of primary metamorphic plagioclase, temperatures were not calculated for samples KB, KM, and KN.

AMPHIBOLITE PETROGRAPHY AND MINERAL GEOCHEMISTRY

Rock Types

Based upon the primary metamorphic mineral compositions and textural characteristics revealed by QEMSCAN[®] and petrographical analyses, three types of amphibolite were distinguished: (1) garnet amphibolite (sample KF, Fig. 4a), (2) clinopyroxene amphibolite (samples KD and KO, Fig. 4b), and (3) common amphibolite (samples KA, KB, KL, KM, and KN, Fig. 4c). All the amphibolite types are partly overprinted by retrograde features as coronas and pseudomorphs, fine-grained aggregates and vein fillings.

Garnet amphibolite

QEMSCAN[®] modal mineralogy shows that this type of amphibolite dominantly consists of nematoblastic amphibole (here referred as hornblende, ~ 65%) and albite (~ 15%) (Fig. 5a), with minor clinopyroxene (Fig. 6a), titanite (Fig. 5a) and kelyphitic garnet (Fig. 5b). The secondary phases are tremolite-actinolite, pumpellyite, prehnite (Fig. 6b), clinozoisite (Fig. 5c), muscovite and chlorite (Fig. 6c).

A complete mineral list is given in Fig. 4a, named as assemblage A (Hbl + Grt + Pl ± Ep-Czo).

Garnet porphyroblasts often show up to 500 μm wide kelyphitic rim (Fig. 4a-inset, Fig. 5b) in a matrix dominated by prismatic hornblende (~ 0.5-2 mm, Fig. 5a). Grains of clinopyroxene are largely replaced by hornblende as demonstrated by segmented and insular appearance of the former (Fig. 6a). The saw-tooth or comb-like interfaces of clinopyroxene fragments point to an intrinsic instability of clinopyroxene under the metamorphic conditions of amphibolite facies, suggesting a possible relict magmatic origin. Plagioclase occurs as small interstitial grains completely pseudomorphosed by albite. Xenoblastic garnet porphyroblasts are normally deformed and contain inclusions of plagioclase (albite) and amphibole.

Retrograde metamorphism has heterogeneously overprinted the prograde assemblage as evidenced by secondary coronas around garnet and amphibole. Garnet breakdown gave rise to a mixture of secondary minerals consisting primarily of fine-grained muscovite, amphibole, pseudomorphosed albitic plagioclase, and chlorite (Figs. 4a-inset, 5b, 6c; hereafter named as assemblage B (Amp + Mu + Ab ± Chl)). Sporadically lenticular to elongate mineral consisting of intimate interlayering of 10-Å mica and Fe-rich 14-Å chlorite (Fig. 6c) occur in kelyphitic coronas. Such appearance is indicative to “metamorphic vermiculite” (or “hydrobiotite”), reported only rarely either from schistose rocks formed at medium temperatures (< 500°C) and low pressures (Ruiz Cruz, 2003) or from ancient and experimental ceramics (Rathossi and Pontikes, 2010; Šegvić et al., 2012). Hornblende is commonly rimmed by retrograde tremolite-actinolite that eventually replaces the entire grains of primary amphibole (Fig. 5b). Secondary lenses were frequently reported in this type of amphibolite consisting exclusively of prehnite and clinozoisite with some minor albite and chlorite (Fig. 6c).

Clinopyroxene amphibolite

Clinopyroxene amphibolites are fine grained and greenish in colour. They contain about 35% hornblende, 35% plagioclase, 15% epidote, and 10% augite (Figs. 5d, 6e). Minor phases are titanite, K-feldspar, chlorite, titanite, apatite, and spinel minerals (Fig. 6d-f). A complete mineral list with respective abundances is provided in Fig. 4b. This assemblage is named assemblage C (Hbl + Pl + Ep + Cpx ± Ttn ± Kfs ± Ap). Green hornblende, generally 0.5-1.5 mm in size, defines a nematoblastic texture in which plagioclase is an interstitial phase. The latter is found partly replaced by albite. An important feature of these rocks is the presence of elongate, xenomorphic clinopyroxene crystals (Fig. 5d) and a high proportion of fine-grained, granular epidote (Fig. 5e). Full crystal shapes of clinopyroxene as well as numerous inclusions of amphibolite paragenesis minerals such as titanite and hornblende (Figs. 5d, 6f) are in favour of a metamorphic origin of clinopyroxene that was originally equilibrated with the amphibolitic mineral assemblage. The epidote may be preserved within the crystalloblasts of hornblende (Fig. 6d, sample KD) or may occur as isometric granular blasts. Textural evidences therefore suggest that the epidote belongs to the prograde metamorphic sequence. Titanite blasts (Fig. 5d) are ubiquitous and are locally accompanied by ilmenite.

Some strongly banded clinopyroxene-bearing amphibolites are also recognized in this group as shown in Fig. 4b. They are characterized by layers of medium-grained amphibole and plagioclase (Fig. 4b-upper inset) and layers composed of fine-grained nematoblastic amphibole, isometric blasts of clinopyroxene and epidote, and plagioclase (Fig. 4b-lower inset). Both types of layers are generally 1-3 cm thick and clearly define the foliation.

Common amphibolite

Common amphibolites are fine-grained with a typical “salt and pepper” appearance in hand specimen caused by white and black flakes present in the rock. These amphibolites are mostly epidote-rich (Fig. 6g), and in the example shown in Fig. 4c, the modal mineralogy consists of hornblende and epidote (~ 35%), plagioclase (~ 15%), and minor chlorite, titanite, calcite, and apatite. This paragenesis is hereafter referred as assemblage D (Hbl + Ep + Pl ± Chl ± Ttn ± Ap). The rock shows domains rich in plagioclase + amphibole and amphibole + epidote, respectively (Fig. 4c inset). The rock texture is clearly nematoblastic outlined by fine-grained (0.5-2 mm) amphibole, granular epidote, and interstitial plagioclase.

Common amphibolites have significantly higher average contents of granular isometric blasts of epidote (up to 2 mm across) than other varieties but it does not appear in all specimens. Epidote readily encloses smaller grains of hornblende, titanite and apatite and frequently shows signs of alterations in tremolite-actinolite and chlorite (Fig. 6g). Epidote blasts appear to be unstable (fracturation, decomposition, and secondary overgrowing) probably due to its rapid prograde growth that eventually faced a disequilibrium at somewhat higher metamorphic conditions (Arnason et al., 1993). Plagioclase is normally found completely replaced by albite. Euhedral grains of titanite, 0.5-3 mm long, are common in all samples but may be partly associated with ilmenite. Evidences of retrograde metamorphism are ubiquitous, numbering mostly chlorite and secondary tremolite-actinolite, which form at the expense of hornblende and epidote (Fig. 5f).

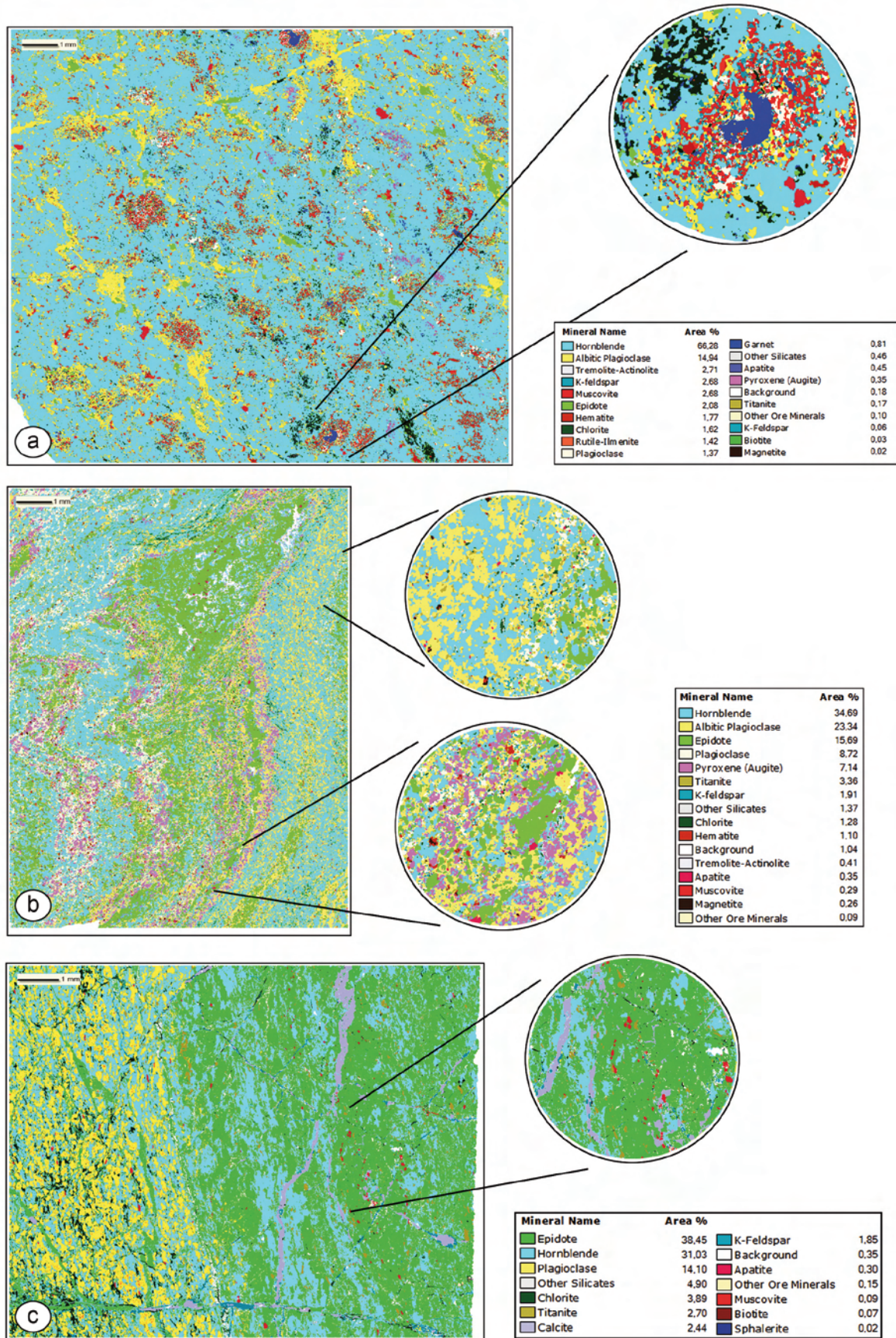


Fig. 4 - QEMSCAN® fieldscan images of different petrographic types of Kalnik Mt. amphibolites depicting their modal mineralogy (in area %) and textural characteristics. (a) Garnet amphibolite (sample KF). The image inset shows a garnet porphyroblast with a corona of muscovite, secondary amphibole, albite and minor chlorite. (b) Clinopyroxene amphibolite (sample KO). The upper image inset shows a band of medium-grained amphibole with plagioclase, whilst the lower one defines a band consisted of fine-grained nematoblastic amphibole, isometric blasts of clinopyroxene and epidote, and plagioclase. (c) Common amphibolite (sample KB). The image inset shows a rock domain rich in amphibole and epidote with some minor phases scattered throughout.

Fractures and veins

All three types of amphibolite contain retrograde cataclastic fractures and veins. The veins consist mainly of cal-

cite and some minor silicate phases, such as prehnite and albite (Figs. 4c, 5f, 6h). This paragenesis is represented by the assemblage E ($\text{Prh} + \text{Ab} \pm \text{Chl} \pm \text{Ep}$).

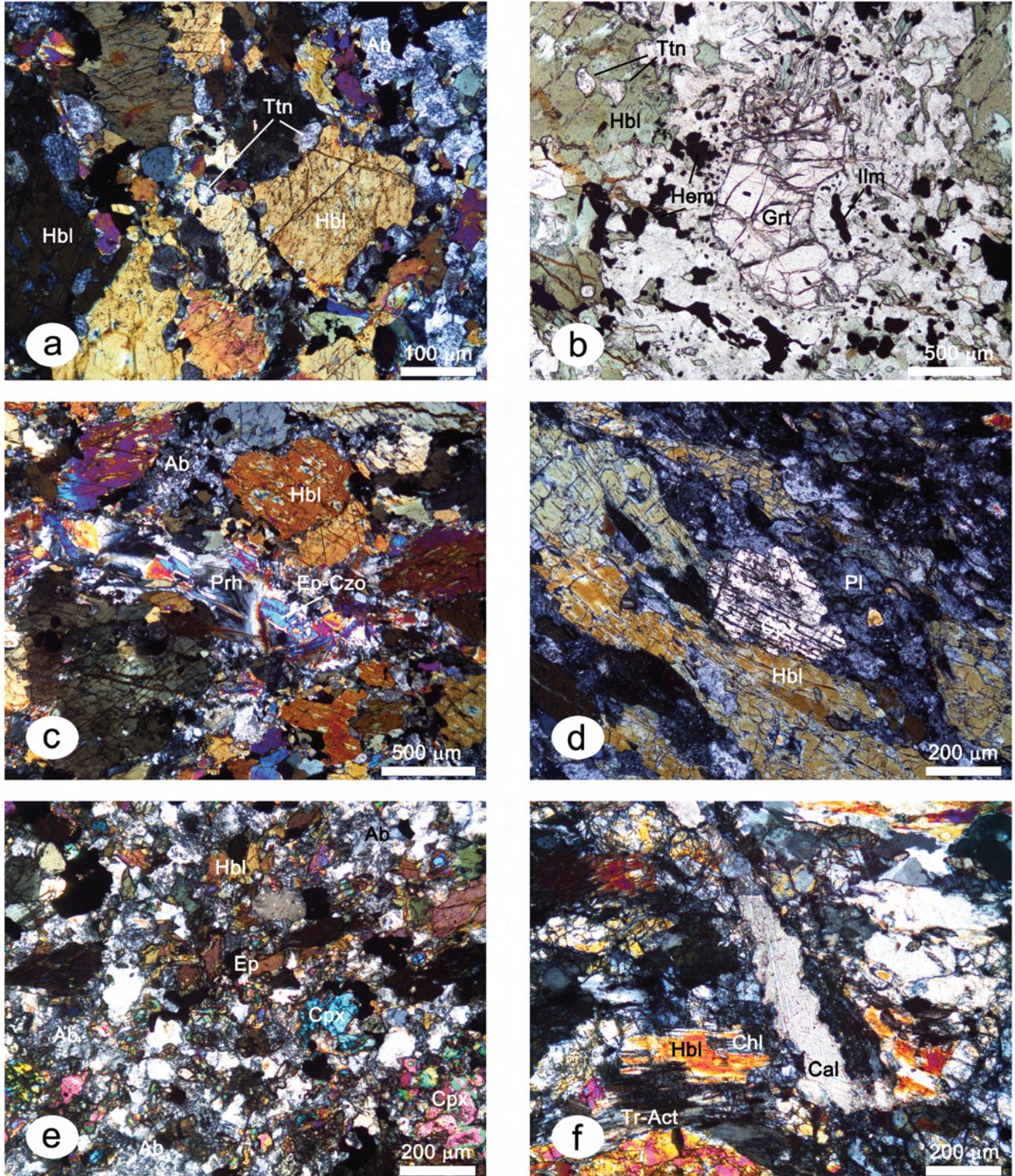


Fig. 5 - Microphotographs of Kalnik Mt. amphibolites thin sections obtained under polarized light. For details see the text. Hb- hornblende, Ttn- titanite, Hem- hematite, Grt- garnet, Ilm- ilmenite, Ab- albite, Prh- prehnite, Ep- epidote, Cz- clinozoisite, Pl- plagioclase, Cpx- clinopyroxene, Chl- chlorite, Tr- tremolite, Act- actinolite, Cal- calcite, Pmp- pumpellyite, Bt- biotite, Ms- muscovite. Mineral abbreviations after Whitney and Evans (2010).

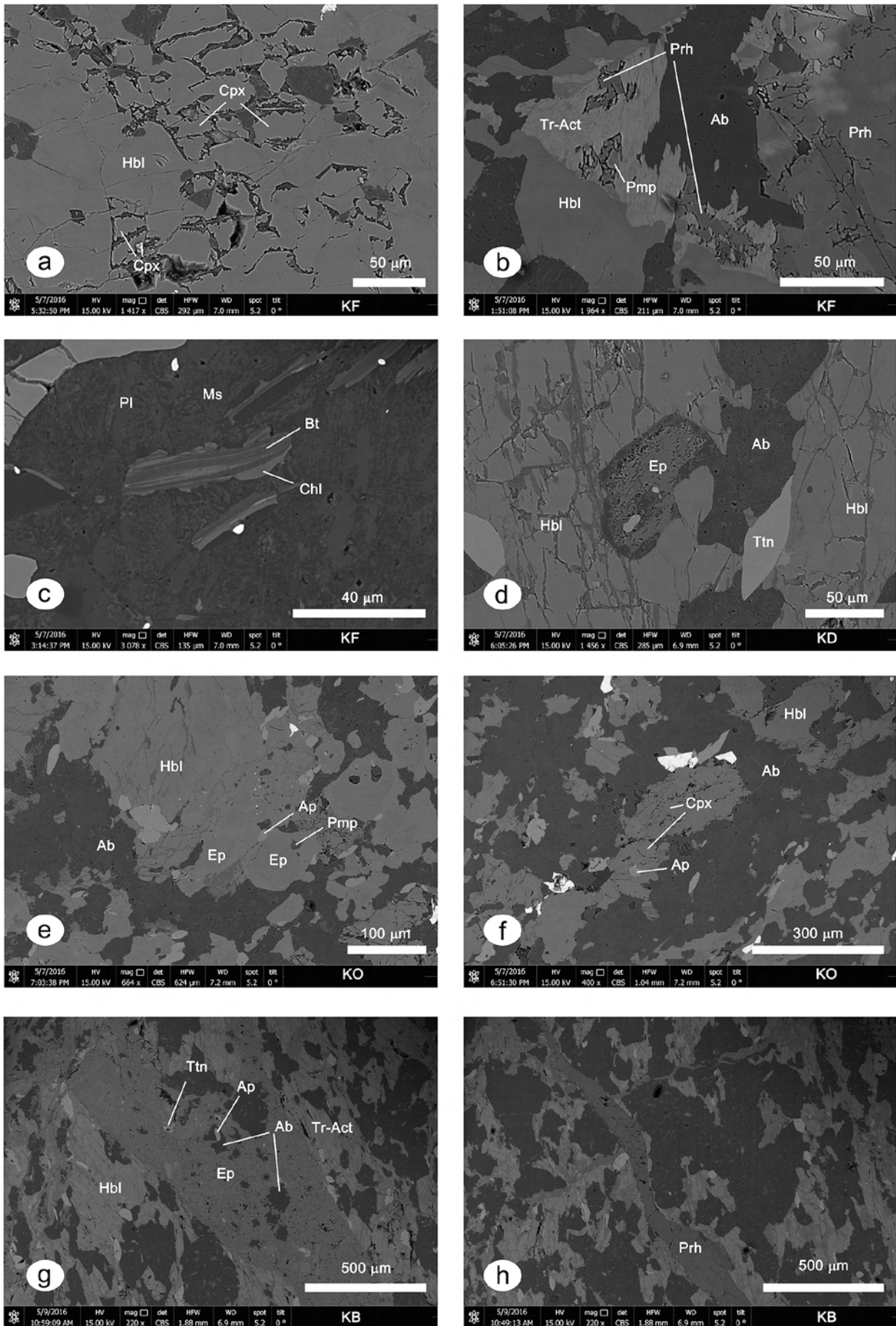


Fig. 6 - SEM back-scattered electron imagery of Kalnik Mt. amphibolites obtained under different magnifications. For details see the text. Mineral abbreviations as in Fig. 5.

Mineral Chemistry

Feldspar

Selected feldspar compositions are shown in Table 1 and plotted in the classification diagram Fig. 7a. Feldspars are represented by albite, peristerite, plagioclase, and alkali feldspar. Plagioclase occurs in samples KD, KF and KO, having a generally homogeneous composition within a sin-

gle crystal. In the samples KD and KF plagioclase is andesine ($An_{30.9-48.6}$), whilst in the sample KO it contains oligoclase ($An_{14.4-29.8}$). Albite and peristerite are reported from (1) kelyphite around garnet, (2) secondary veins, and (3) inclusions in amphibole. Their overall composition is $Ab_{84.2-99.4}Or_{0.1-5}An_{0.2-14.2}$. Alkali feldspar ($Ab_{13.1}Or_{86.9}An_{0.00}$) is reported only in the KO sample.

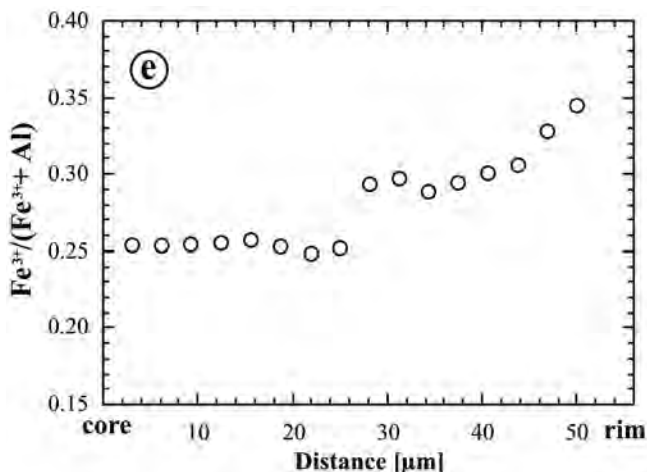
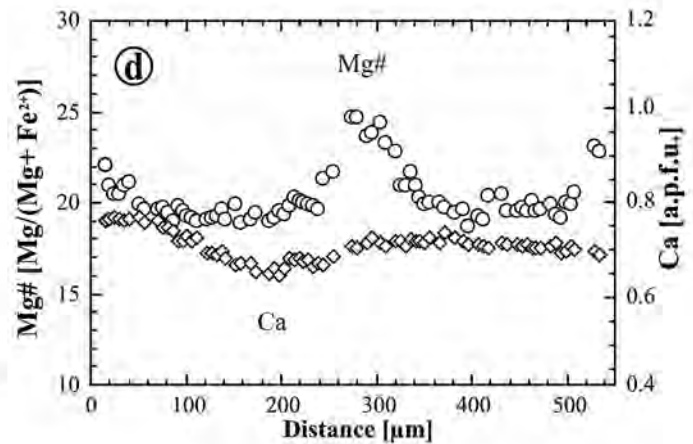
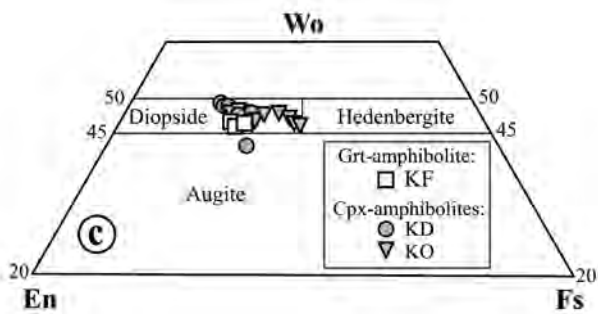
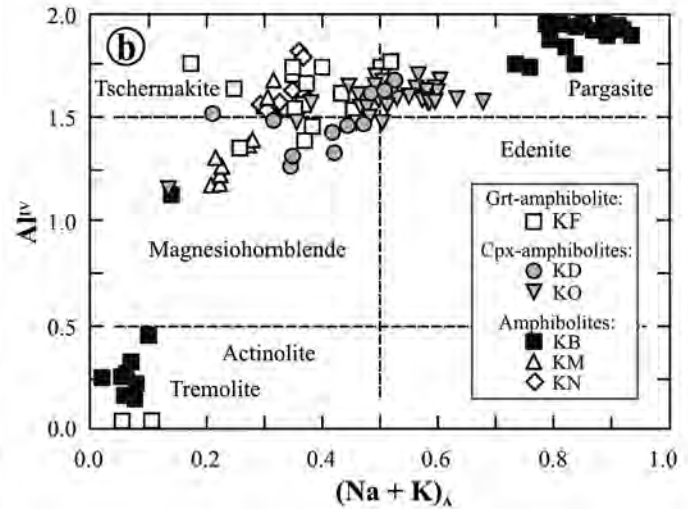
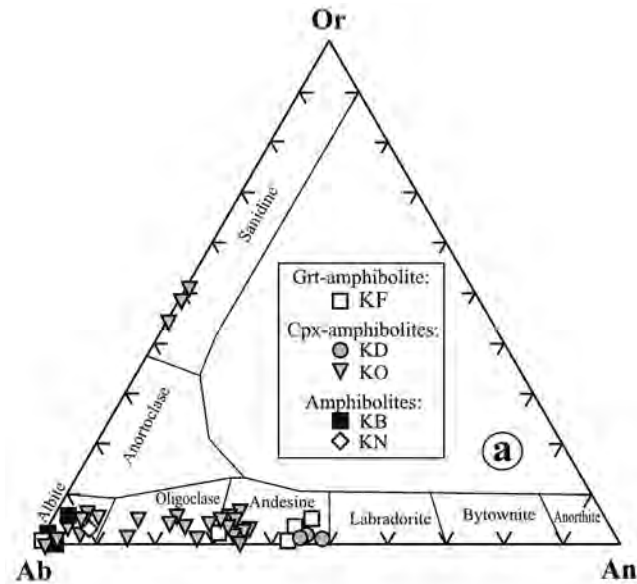


Fig. 7 - (a) Plot of feldspar compositions in the Ab-An-Or diagram for amphibolites from Kalnik Mt. metamorphic sole. (b) $Al^{IV}-(Na + K)_A$ plot of amphiboles using the classification of Leake et al. (1997). (c) Plot of clinopyroxene compositions in the En-Wo-Fs ($Mg_2Si_2O_6-Ca_2Si_2O_6-Fe_2Si_2O_6$) diagram with the nomenclature fields of Morimoto (1988). (d) Variation of Mg# along the garnet porphyroblast in a garnet-clinopyroxene amphibolite sample KF. (e) Variation of $Fe^{3+}/(Fe^{3+} + Al)$ along the epidote in a clinopyroxene amphibolite sample KO.

Table 1. Selected microprobe analyses and formulae of feldspars from the Kalnik Mt. amphibolites.

Sample Anal. No.	KF 10	KF 24	KF 52	KD 04	KD 33	KO 08	KO 54	KO 58	KB 41	KO 11	KO 12	KO 13
SiO ₂	56.83	60.78	68.60	56.58	55.64	64.77	63.42	61.33	68.42	61.81	62.37	60.32
Al ₂ O ₃	26.83	25.42	18.97	28.30	28.78	20.75	22.37	24.37	19.42	25.17	24.72	25.53
Fe ₂ O ₃	0.20	0.25	0.31	0.43	0.33	2.14	0.92	0.68	0.06	0.22	0.22	0.19
BaO	0.00	0.00	0.00	0.00	0.00	0.00	0.00	0.00	0.00	0.36	0.36	0.30
CaO	9.27	6.24	0.02	9.28	10.04	1.10	2.94	4.16	0.08	0.00	0.00	0.00
Na ₂ O	6.37	7.92	12.00	6.16	5.76	10.26	9.13	7.99	11.69	5.58	5.30	6.35
K ₂ O	0.13	0.32	0.03	0.22	0.17	0.47	0.84	0.89	0.05	8.00	8.36	7.60
Total	99.63	100.92	99.92	100.98	100.72	99.48	99.61	99.42	99.72	101.13	101.32	100.29
Si	2.56	2.68	3.00	2.52	2.49	2.88	2.82	2.75	3.00	2.76	2.78	2.72
Al	1.43	1.32	0.98	1.48	1.52	1.09	1.17	1.28	1.00	1.33	1.30	1.36
Fe ³⁺	0.01	0.01	0.01	0.01	0.01	0.07	0.03	0.02	0.00	0.01	0.01	0.01
Ba	0.00	0.00	0.00	0.00	0.00	0.00	0.00	0.00	0.00	0.01	0.01	0.01
Ca	0.45	0.29	0.00	0.44	0.48	0.05	0.14	0.20	0.00	0.00	0.00	0.00
Na	0.56	0.68	1.02	0.53	0.50	0.88	0.79	0.69	0.99	0.48	0.46	0.51
K	0.01	0.02	0.00	0.01	0.01	0.03	0.05	0.05	0.00	0.46	0.48	0.44
Total	5.02	5.00	5.01	4.99	5.01	5.00	5.00	4.99	4.99	5.05	5.04	5.05
Or	0.70	1.80	0.10	1.30	1.00	2.80	4.90	5.40	0.30	48.60	50.90	44.00
Ab	55.00	68.41	99.78	53.88	50.46	91.75	80.69	73.47	99.32	51.45	49.06	55.96
An	44.26	29.77	0.07	44.84	48.56	5.45	14.38	21.12	0.38	0.00	0.00	0.00

Formulae calculated on the basis of 8 oxygens and all Fe as Fe³⁺. End members are in molar %: Or = 100*K/(Ca+Na+K), An = 100*Ca/(Ca+Na+K), Ab = 100*Na/(Ca+Na+K). KF – garnet amphibolite, KD and KO – clinopyroxene amphibolites, KB – common amphibolites.

Amphibole

Selected amphibole compositions are shown in Table 2 and plotted in the classification diagram Fig. 7b. According to the classification of Leake et al. (1997), all analysed amphiboles are calcic with a broad compositional range. In the garnet amphibolites the amphibole is mostly tschermakite ($Ca_B = 1.665-1.908$ a.p.f.u.; $Ti = 0.037-0.197$ a.p.f.u.; $Mg\# [Mg/(Mg+Fe^{2+})] = 54.904-62.619$), whilst in Cpx-amphibolite the amphibole has composition close to the magnesiohornblende-tschermakite-pargasite transition ($Ca_B = 1.812-1.966$ a.p.f.u.; $Ti = 0.043-0.104$ a.p.f.u.; $Mg\# [Mg/(Mg+Fe^{2+})] = 50.522-59.778$). Amphibole from common amphibolites is either pargasite or retrograde tremolite (sample KB: $Ca_B = 1.723-1.974$ a.p.f.u.; $Ti = 0.000-0.172$ a.p.f.u.; $Mg\# [Mg/(Mg+Fe^{2+})] = 50.207-66.708$), otherwise having the composition of magnesiohornblende to tschermakite ($Ca_B = 1.801-1.849$ a.p.f.u.; $Ti = 0.087-0.134$ a.p.f.u.; $Mg\# [Mg/(Mg+Fe^{2+})] = 54.04-64.167$).

The compositional variations of the analysed amphiboles are essentially controlled by pargasitic substitution vector. This implies a temperature-controlled metamorphism wherein the contents of tetrahedral Al and Na in amphibole site A are highly correlated. The dominant pargasitic substitution trend is not documented by the raise of alumina content toward the grain rims, normally taken as a sign of prograde metamorphism (Raase et al., 1986). Hence, a certain degree of post-peak re-equilibration of amphibole geochemistry must have taken place.

Clinopyroxene

Selected clinopyroxene compositions are shown in Table 2 and plotted in the classification diagram of Fig. 7c., where they fall within the field of diopside (Morimoto, 1988). The overall compositional range of clinopyroxene is 42.4-49.8 wt% Wo, 27.1-36.8 wt% En, and 13.8-26.2 wt% Fs. The $Mg\#$ values vary between 59.2 and 77.9, whereas the total alumina content is approximately 2 wt %. The Tschermak enrichment typical for clinopyroxene from high-grade metamorphic facies is not observed ($Al^{VI}/Al^{IV} \sim 0.14-0.79$) hence suggesting moderate pressures of metamorphism (e.g., Mukhopadhyay, 1991). Clinopyroxene has relatively homogeneous compositions. Zoning is developed next to reaction coronas and at the overgrowing grains periphery. The zoning pattern is analogue to that of amphibole, testified by by Al_2O_3 decrease and increase of Si, Ca and $Mg\#$ towards grain boundaries, which is typical for cooling and decompression (Deer et al., 1996).

Garnet

Selected chemical analyses and formulas of garnet are shown in Table 2. Garnet bulk compositional range is $Py_{10.2-17.1}Alm_{51.9-57.8}Sp_{5.3-9.0}Gr_{15.8-25.4}And_{2.4-6.6}$ with uvarovite and melanite component as low as 0.3 mole% and 0.8 mole%, respectively. Large garnet porphyroblasts are composite grains of two or three overgrown blasts ($\sim 500 \mu m$). Microprobe profiles across two garnet porphyroblasts reveal different compositional zoning patterns. In Fig. 7d, a composite grain

Table 2. Selected microprobe analyses and formulae of garnet, amphibole and clinopyroxene from the Kalnik Mt. amphibolites.

Sample Anal. No. Remarks	Garnet										Clinopyroxene										Amphibole																											
	KF 40#1		KF 4#1		KF 34#2		KF 2#2		KF 38#3		KF 34		KO 02		KO 90		KO 497#3		KO 506#3		KF 25		KO 51		KD 22		KD 20		KB 04		KB 15		KM 03		KN 20													
	core	rim	core	rim	core	rim	core	rim	core	rim	core	rim	core	rim	core	rim	core	rim	core	rim	core	rim	core	rim	core	rim	core	rim	core	rim	core	rim	core	rim	core	rim												
SiO ₂	37.87	37.54	37.60	37.64	37.63	37.63	37.64	37.63	37.63	51.69	50.36	52.12	51.08	51.53	41.82	41.52	42.19	44.90	39.65	53.88	43.16	46.63	43.14	37.87	37.54	37.60	37.64	37.63	37.63	37.64	37.63	37.63	51.69	50.36	52.12	51.08	51.53	41.82	41.52	42.19	44.90	39.65	53.88	43.16	46.63	43.14		
TiO ₂	0.07	0.12	0.14	0.13	0.22	0.22	0.18	0.08	0.04	0.18	0.08	0.04	0.11	0.14	1.74	0.77	0.89	0.64	1.40	0.02	0.02	1.05	0.78	1.04	0.07	0.12	0.14	0.13	0.22	0.22	0.18	0.08	0.04	0.18	0.08	0.04	0.11	0.14	1.74	0.77	0.89	0.64	1.40	0.02	0.02	1.05	0.78	1.04
Al ₂ O ₃	20.82	20.71	20.41	20.49	20.22	20.22	1.77	2.11	1.34	2.12	2.01	12.36	11.98	12.54	8.93	12.92	13.55	12.46	8.55	12.72	20.82	20.71	20.41	20.49	20.22	20.22	1.77	2.11	1.34	2.12	2.01	12.36	11.98	12.54	8.93	12.92	13.55	12.46	8.55	12.72								
Cr ₂ O ₃	0.00	0.08	0.00	0.01	0.02	0.06	0.04	0.02	0.03	0.04	0.06	0.05	0.05	0.05	0.05	0.05	0.05	0.10	0.07	0.01	0.10	0.10	0.08	0.00	0.08	0.00	0.01	0.02	0.06	0.04	0.02	0.03	0.04	0.06	0.05	0.05	0.05	0.05	0.05	0.05	0.10	0.07	0.01	0.10	0.10	0.08		
Fe ₂ O ₃	0.79	1.79	1.74	1.35	0.97	2.53	4.44	3.41	2.79	2.07	1.30	3.90	1.84	3.47	1.57	0.00	2.11	1.53	1.62	0.79	1.79	1.74	1.35	0.97	2.53	4.44	3.41	2.79	2.07	1.30	3.90	1.84	3.47	1.57	0.00	2.11	1.53	1.62										
FeO	24.37	25.82	24.97	24.28	24.26	8.15	11.09	6.32	7.44	7.57	15.01	13.94	15.63	16.18	13.83	14.78	14.07	12.63	24.37	25.82	24.97	24.28	24.26	8.15	11.09	6.32	7.44	7.57	15.01	13.94	15.63	16.18	13.83	14.78	14.07	12.63												
MnO	2.59	3.09	2.77	2.58	3.98	0.32	0.49	0.45	0.38	0.34	0.27	0.56	0.36	0.25	0.34	0.40	0.36	0.23	2.59	3.09	2.77	2.58	3.98	0.32	0.49	0.45	0.38	0.34	0.27	0.56	0.36	0.25	0.34	0.40	0.36	0.23												
MgO	3.84	3.51	2.63	2.91	3.04	12.51	9.05	12.52	11.71	12.23	10.49	9.98	9.59	11.40	9.61	14.62	10.61	12.06	3.84	3.51	2.63	2.91	3.04	12.51	9.05	12.52	11.71	12.23	10.49	9.98	9.59	11.40	9.61	14.62	10.61	12.06												
CaO	8.98	7.66	9.85	10.19	8.96	22.86	21.63	23.81	23.49	23.22	11.65	11.91	11.81	12.06	11.53	12.64	11.45	11.50	8.98	7.66	9.85	10.19	8.96	22.86	21.63	23.81	23.49	23.22	11.65	11.91	11.81	12.06	11.53	12.64	11.45	11.50												
Na ₂ O	-	-	-	-	-	0.41	1.05	0.59	0.51	0.49	1.75	1.55	1.48	1.10	2.12	0.30	1.66	1.17	1.85	-	-	-	-	-	0.41	1.05	0.59	0.51	0.49	1.75	1.55	1.48	1.10	2.12	0.30	1.66	1.17	1.85										
K ₂ O	-	-	-	-	-	-	-	-	-	-	0.80	0.99	0.96	0.56	1.74	0.08	0.27	0.18	0.24	-	-	-	-	-	0.80	0.99	0.96	0.56	1.74	0.08	0.27	0.18	0.24															
H ₂ O	-	-	-	-	-	-	-	-	-	-	1.99	1.98	2.00	1.99	1.95	2.06	2.02	2.02	-	-	-	-	-	1.99	1.98	2.00	1.99	1.95	2.06	2.02	2.02																	
Total	99.33	100.30	100.09	99.57	99.30	100.47	100.34	100.63	99.65	99.62	99.26	99.13	99.34	99.10	99.13	99.19	99.95	99.41	99.13	99.33	100.30	100.09	99.57	99.30	100.47	100.34	100.63	99.65	99.62	99.26	99.13	99.34	99.10	99.13	99.19	99.95	99.41	99.13										
Si	2.999	2.972	2.996	3.000	3.003	1.934	1.925	1.943	1.929	1.940	6.296	6.294	6.367	6.724	6.087	7.854	6.410	6.893	6.391	2.999	2.972	2.996	3.000	3.003	1.934	1.925	1.943	1.929	1.940	6.296	6.294	6.367	6.724	6.087	7.854	6.410	6.893	6.391										
Al ^{IV}	0.001	0.028	0.004	0.000	0.000	0.066	0.075	0.057	0.071	0.060	1.704	1.706	1.633	1.276	1.913	0.146	1.590	1.107	1.609	0.001	0.028	0.004	0.000	0.000	0.066	0.075	0.057	0.071	0.060	1.704	1.706	1.633	1.276	1.913	0.146	1.590	1.107	1.609										
Al ^{VI}	1.944	1.903	1.913	1.923	1.903	0.013	0.020	0.002	0.023	0.029	0.490	0.434	0.597	0.301	0.425	0.085	0.590	0.383	0.612	1.944	1.903	1.913	1.923	1.903	0.013	0.020	0.002	0.023	0.029	0.490	0.434	0.597	0.301	0.425	0.085	0.590	0.383	0.612										
Ti	0.004	0.007	0.008	0.008	0.013	0.005	0.002	0.001	0.003	0.004	0.197	0.087	0.101	0.072	0.161	0.002	0.117	0.087	0.116	0.004	0.007	0.008	0.008	0.013	0.005	0.002	0.001	0.003	0.004	0.197	0.087	0.101	0.072	0.161	0.002	0.117	0.087	0.116										
Cr	0.000	0.005	0.002	0.000	0.001	0.002	0.001	0.001	0.001	0.001	0.007	0.006	0.006	0.012	0.014	0.008	0.001	0.012	0.009	0.000	0.005	0.002	0.000	0.001	0.002	0.001	0.001	0.001	0.001	0.007	0.006	0.006	0.012	0.014	0.008	0.001	0.012	0.009										
Fe ³⁺	0.056	0.113	0.087	0.075	0.067	0.071	0.128	0.096	0.079	0.059	0.149	0.445	0.209	0.391	0.181	0.000	0.236	0.170	0.181	0.056	0.113	0.087	0.075	0.067	0.071	0.128	0.096	0.079	0.059	0.149	0.445	0.209	0.391	0.181	0.000	0.236	0.170	0.181										
Fe ²⁺	1.606	1.703	1.642	1.640	1.615	2.255	0.354	0.197	0.235	0.238	1.890	1.767	1.973	1.713	2.078	1.686	1.836	1.740	1.565	1.606	1.703	1.642	1.640	1.615	2.255	0.354	0.197	0.235	0.238	1.890	1.767	1.973	1.713	2.078	1.686	1.836	1.740	1.565										
Mn	0.174	0.207	0.184	0.160	0.269	0.010	0.016	0.014	0.012	0.011	0.035	0.071	0.046	0.031	0.044	0.042	0.050	0.045	0.029	0.174	0.207	0.184	0.160	0.269	0.010	0.016	0.014	0.012	0.011	0.035	0.071	0.046	0.031	0.044	0.042	0.050	0.045	0.029										
Mg	0.454	0.414	0.304	0.361	0.362	0.698	0.516	0.696	0.659	0.686	2.335	2.255	2.158	2.545	2.200	3.178	2.349	2.697	2.663	0.454	0.414	0.304	0.361	0.362	0.698	0.516	0.696	0.659	0.686	2.335	2.255	2.158	2.545	2.200	3.178	2.349	2.697	2.663										
Ca	0.762	0.649	0.859	0.834	0.767	0.917	0.886	0.951	0.950	0.936	1.879	1.934	1.909	1.935	1.896	1.974	1.821	1.867	1.825	0.762	0.649	0.859	0.834	0.767	0.917	0.886	0.951	0.950	0.936	1.879	1.934	1.909	1.935	1.896	1.974	1.821	1.867	1.825										
Na	-	-	-	-	-	0.030	0.077	0.043	0.038	0.036	0.511	0.455	0.434	0.320	0.631	0.086	0.477	0.334	0.530	-	-	-	-	-	0.030	0.077	0.043	0.038	0.036	0.511	0.455	0.434	0.320	0.631	0.086	0.477	0.334	0.530										
K	-	-	-	-	-	-	-	-	-	-	0.154	0.191	0.184	0.108	0.340	0.015	0.051	0.034	0.046	-	-	-	-	-	0.154	0.191	0.184	0.108	0.340	0.015	0.051	0.034	0.046															

Garnet formulae calculated on basis of 12 oxygens and 8 cations. # corresponds to discrete garnet porphyroblast. Clinopyroxene formulae calculated on the basis of 6 oxygens and 4 cations. Amphibole formulae calculated on the basis of 23 oxygens and 15 cations excluding Na and K; H₂O is value corresponding to 1(OH) p.f.u. KF – garnet amphibolite, KD and KO – clinopyroxene amphibolite, KB, KM and KN – common amphibolite. sec = secondary paragenesis.

profile of two blasts displays a slight core to rim increase in the pyrope component at the expense of the almandine component. The second profile of a single blast of garnet reveals a faint zonation with a grossularite component increasing towards the rims. Generally, the flat profile patterns suggest garnet equilibration and homogenisation by cation volume diffusion under peak P-T conditions of metamorphism (e.g., Woodsworth, 1977). However, the slight “U” shape of pyrope concentration pattern, accompanied by an opposite trend of almandine and spessartine abundances should imply a prograde metamorphic event (e.g., Romano et al., 2006).

Epidote

Epidote is reported from samples KO and KB. Selected compositions are shown in Table 3. Epidote typically occurs in form of aggregated mineral clusters or as discrete idiomorphic to xenoblastic grains which are strongly zoned with Fe-poor rims and Fe-rich cores. This is depicted in Fig. 7e, wherein the $X_{\text{Fe}} = [\text{Fe}^{3+}/(\text{Fe}^{3+} + \text{Al})]$ ratio is approximately 0.25 at the core, whilst toward rims it achieves a value of 0.29. A zoning of this kind is a characteristic feature of prograde epidote growth under low to medium grade metamorphic conditions (Beiersdorf and Day, 1995).

Other minerals

Selected *chlorite* compositions are shown in Table 3. Total cation number is found to be slightly below 10, suggesting a dominant presence of divalent iron, thus classifying the analysed chlorites as trioctahedral. The Kalnik Mt. chlorites are present in all types of amphibolite and have a retrograde origin. According to Hey (1954) the analysed chlorite is dominantly pycnochlorite (samples KB and KF: $X_{\text{Fe}} = 45-65$), and less commonly diabantite (samples KD and KO: $X_{\text{Fe}} = 40-45$) and ripidolite (sample KF: $X_{\text{Fe}} = 85$).

Selected *titanite* compositions are shown in Table 3. Titanite is generally Al-rich (up to 3.96 wt% Al_2O_3) with moderate Fe contents (up to 3.39 wt% Fe_2O_3). Titanium varies from 0.78 to 0.97 a.p.f.u., indicating a variable substitution according to $(\text{Al}, \text{Fe}^{3+}) + (\text{OH}, \text{F}) \leftrightarrow \text{Ti}^{4+} + \text{O}^{2-}$. However, data shows that in most titanites the Ti content reaches the maximum per formula unit, which is attributed to high grade metamorphic conditions and titanite prograde origin (Higgins and Ribbe, 1976). Commonly, such titanite emerges as an isometric medium-sized ($\sim 30-50 \mu\text{m}$) inclusion in amphiboles and pyroxenes or, rarely, forms ellipsoidal blebs. A low-Ti titanite (~ 0.77 a.p.f.u.) is only reported from the sample KF, where it occurs as inclusion in amphiboles accompanied by ilmenite. According to Harlov et al. (2006) ilmenite may produce titanite via retrograde hydration and oxidation through reactions with clinopyroxene and amphibole, respectively.

Minor and accessory silicate phases observed either in matrix, veins, or as inclusions are prehnite, Fe-pumpellyite, and muscovite (white mica). Their compositions are shown in Table 3. *Prehnite* and *pumpellyite* occur as secondary phases formed after plagioclase dissolution, whilst *muscovite* is recovered from garnet reaction zone in sample KF (assemblage B). The compositions of minor oxides are shown in Table 4. Ilmenite with higher content of pyrophanite component ($\text{Ilm}_{0.56-0.69}\text{Pfn}_{0.22-0.39}\text{Hem}_{0.07-0.21}$) is reported in samples KF and KN. Another opaque phase reported in the former sample is brookite with a tendency toward the end-member ferro-pseudobrookite composition ($\text{Fe}^{2+}_{0.524-0.753}\text{Fe}^{3+}_{0.437-0.774}\text{Ti}_{1.605-1.780}$).

WHOLE-ROCK GEOCHEMISTRY

Major and trace elements compositions of amphibolites from Kalnik Mt. are given in Table 5. All the rocks are characterized by relatively uniform contents of SiO_2 (43.56-48.49 wt%) and Al_2O_3 (13.24-15.49 wt%) typical of basaltic rocks. The CaO abundances are low to moderate (8-14 wt%), with X_{Mg} varying between 50.8 and 65.8. Potassium amounts (0.43-1.79 wt%) is consistent with metabasite protholiths, whereas somewhat higher content of Na_2O (2.50-3.94 wt%) may reflect post-magmatic modifications. Volatile components ($\text{H}_2\text{O} + \text{CO}_2$) range from ~ 1.6 to 4.7 wt%, being the lowest in Grt-Cpx and Cpx amphibolites, thus reflecting the comparatively higher metamorphic conditions under which these varieties were formed.

Primitive mantle-normalized trace element abundance patterns and chondrite-normalized REE patterns are presented in Fig. 6 (normalisation values after Hofmann, 1988; McDonough and Sun, 1990). All the normalized REE curves show smooth parallel trends with LREE depletion ($(\text{La}_N/\text{Sm}_N = 0.54-0.82)$), nearly flat HREE ($(\text{Tb}_N/\text{Lu}_N = 0.98-1.16)$) at maximum 25 times chondrite abundances (Fig. 8a). Similar REE patterns correspond to those of Normal Mid Ocean Ridge Basalt type (N-MORB-type) oceanic crust originated from a depleted mantle source devoid of any residual garnet (e.g., Wood and Banno, 1973). The majority of analysed amphibolites show a slightly negative Eu anomaly ($\text{Eu}/\text{Eu}^* = 0.91-0.99$), which is characteristic of some fractionation of magmatic plagioclase. Yet, the REE normalized curves of samples KA, KB, and KL (Fig. 8b) are marked by comparatively lower HREE normalized values (maximum 15 times relative to chondrite) and a pronounced positive Eu anomaly ($\text{Eu}/\text{Eu}^* = 1.36-2.22$), which is typical of cumulate gabbroic rocks.

Primitive mantle-normalized trace element concentration diagram of the amphibolites with basaltic and cumulate protholiths are reported in Fig. 8c-d, respectively. All samples show LIL-elements (Rb, Ba, and K) enrichment and moderately flat curve trends for the less incompatible elements. High-field-strength elements (HFSE) show peculiar subduction zone geochemical signatures such as a slight Nb-Ta, as well as P and Ti negative anomalies. The amphibolites with a cumulate imprint displayed by Eu positive anomaly are characterized by Sr enrichment (Fig. 8d) which reinforces the hypothesis of plagioclase-rich gabbroic cumulate protholiths.

DISCUSSION

Nature and geotectonic setting of the igneous protholiths

Apart from the loss of volatile components, metamorphism is considered to be essentially an isochemical process (e.g., Greenfield et al., 1998). In other words, the major and trace element concentrations in metamorphic rocks reflect the composition of their respective protholiths and are of essential importance in petrogenetic considerations. Still, the composition of different metabasites can differ from their protholiths. This may be caused by hydrothermal alteration, weathering and retrograde metamorphism (Vernon and Clarke, 2008). In particular, the LIL elements, such as Cs, Rb, Ba, K, and U, are susceptible to deuteric processes due to their fluid-mobile behaviour (e.g., Rollinson, 1993). The retrograde processes affect the major element concentrations in metamorphic rocks only rarely, usually yielding changes of Fe/Mg ratios or Si depletion. Hence, in this study only the abundances of relatively immobile minor elements such

Table 4. Selected microprobe analyses and formulae of rutile, ilmenite, hematite and Fe-Ti oxide from the Kalnik Mt. amphibolites.

Sample Anal. no. Remark	Rutile		Ilmenite		Hematite				Fe-Ti oxide	
	KF	KF	KN	KF	KO	KO	KM	KN	KN	KN
	50	04	04	29	118	119	13	21	05	26
SiO ₂	0.02	0.02	0.02	0.02	0.00	0.04	0.07	0.08	0.03	0.17
TiO ₂	98.93	46.99	51.06	0.16	0.07	0.51	0.00	0.00	60.44	57.75
Al ₂ O ₃	0.00	0.00	0.00	0.39	0.11	0.07	0.86	0.89	0.00	0.00
Cr ₂ O ₃	0.08	0.09	0.02	0.07	0.04	0.09	0.03	0.03	0.02	0.02
Fe ₂ O ₃	1.37	10.80	3.88	99.76	100.52	99.17	95.73	96.61	14.83	19.76
FeO	0.00	27.09	26.81	0.06	0.00	0.00	0.00	0.00	22.98	18.22
MnO	0.00	14.85	18.55	0.03	0.11	0.19	0.24	0.17	0.50	3.02
MgO	0.00	0.06	0.09	0.00	0.00	0.00	1.04	1.04	0.05	0.06
CaO	0.25	0.03	0.14	0.05	0.02	0.26	0.33	0.20	0.21	0.18
Total	100.65	99.94	100.58	100.56	100.87	100.34	98.31	99.01	99.08	99.19
Si	0.000	0.001	0.001	0.001	0.000	0.001	0.002	0.002	0.001	0.007
Ti	0.987	0.896	0.963	0.003	0.001	0.010	0.000	0.000	1.780	1.702
Al	0.000	0.000	0.000	0.012	0.003	0.002	0.027	0.028	0.000	0.000
Cr	0.001	0.002	0.000	0.002	0.001	0.002	0.001	0.001	0.001	0.001
Fe ³⁺	0.014	0.206	0.073	1.979	1.992	1.973	1.932	1.935	0.437	0.583
Fe ²⁺	0.000	0.574	0.562	0.001	0.000	0.000	0.000	0.000	0.753	0.597
Mn	0.000	0.319	0.394	0.001	0.002	0.004	0.006	0.004	0.017	0.100
Mg	0.000	0.002	0.003	0.000	0.000	0.000	0.042	0.041	0.003	0.004
Ca	0.004	0.001	0.004	0.001	0.001	0.007	0.009	0.006	0.009	0.008
Total	1.005	2.000	2.000	2.000	2.001	2.000	2.018	2.016	3.000	3.000

KF – garnet amphibolite, KD and KO – clinopyroxene amphibolites, KB, KM and KN – common amphibolites.

as high-field strength elements (HFSE) and rare-earth elements (REE) were considered for the purpose of petrogenetic and geotectonic considerations (e.g., Shervais, 1982).

The Ni vs. Mg# relationship in analysed metabasites reveals a broad positive correlation ($r' = 0.76$, Fig. 9a). Such a regular Ni-Mg# trend is encountered in basic magma series produced by variable amounts of olivine fractionation. If any non-igneous processes had affected the basaltic protolith, or the protolith was not a magmatic rock, the Ni-Mg# trend would have not been maintained. This is in agreement with the HFSE ratios, i.e. low and high values of Nb/Y (0.04-0.11) and Zr/Nb (25-35), respectively, and a slight LREE depletion with respect to HREE with $La_N/Yb_N \sim 0.68$ (Fig. 8a-b). Zr/Ti and Nb/Y ratios (Winchester and Floyd, 1977) define the analysed rocks as subalkaline basalts (Fig. 9b). The ratios of incompatible elements like La/Sm and Zr/Nb, insensitive to magmatic differentiation (e.g., Pearce and Peate, 1995), range from 0.9-1.2 and 20.2-35.3, respectively. These values are characteristic of Transitional to Normal MORB magmas (e.g., Mahoney et al., 1993). Based on the Ti/Cr vs. Ni and the discrimination criteria suggested by Beccaluva et al. (1980) on magma affinities in ophiolites,

most of the samples are defined as high-Ti basalts, with the exception of samples KA, KB, and KL, classified as low-Ti basalts. This is considered typical for MORB and SSZ (Supra-subduction Zone) affinity, respectively. Samples classified as low-Ti basalts correspond to those earlier defined as gabbroic metacumulates inferred by their characteristic Eu and Sr anomalies (Fig. 8).

The geochemical evidences presented above enable a classification of magmatic protoliths of the Kalnik Mt. amphibolites into two, genetically related groups. As a whole, the incompatible trace elements suggest MORB affinity of the parental magmas coupled with some minor SSZ influences (Fig. 8). In several discrimination diagrams based on incompatible trace element contents (Fig. 10) these rocks clearly form a SSZ array between MORB and island arc tholeiite (IAT) thus representing the geochemistry of back-arc basin basaltic extrusives (BABB; group of high-Ti metabasalts) and IAT-like intrusives (group of low-Ti metacumulates - samples: KA, KB and KL). It should be noted, however, that the V-Ti/1000 plot (Fig. 10d) has been used for basaltic extrusives only due to the possible enrichment or depletion of Ti in meta-cumulates.

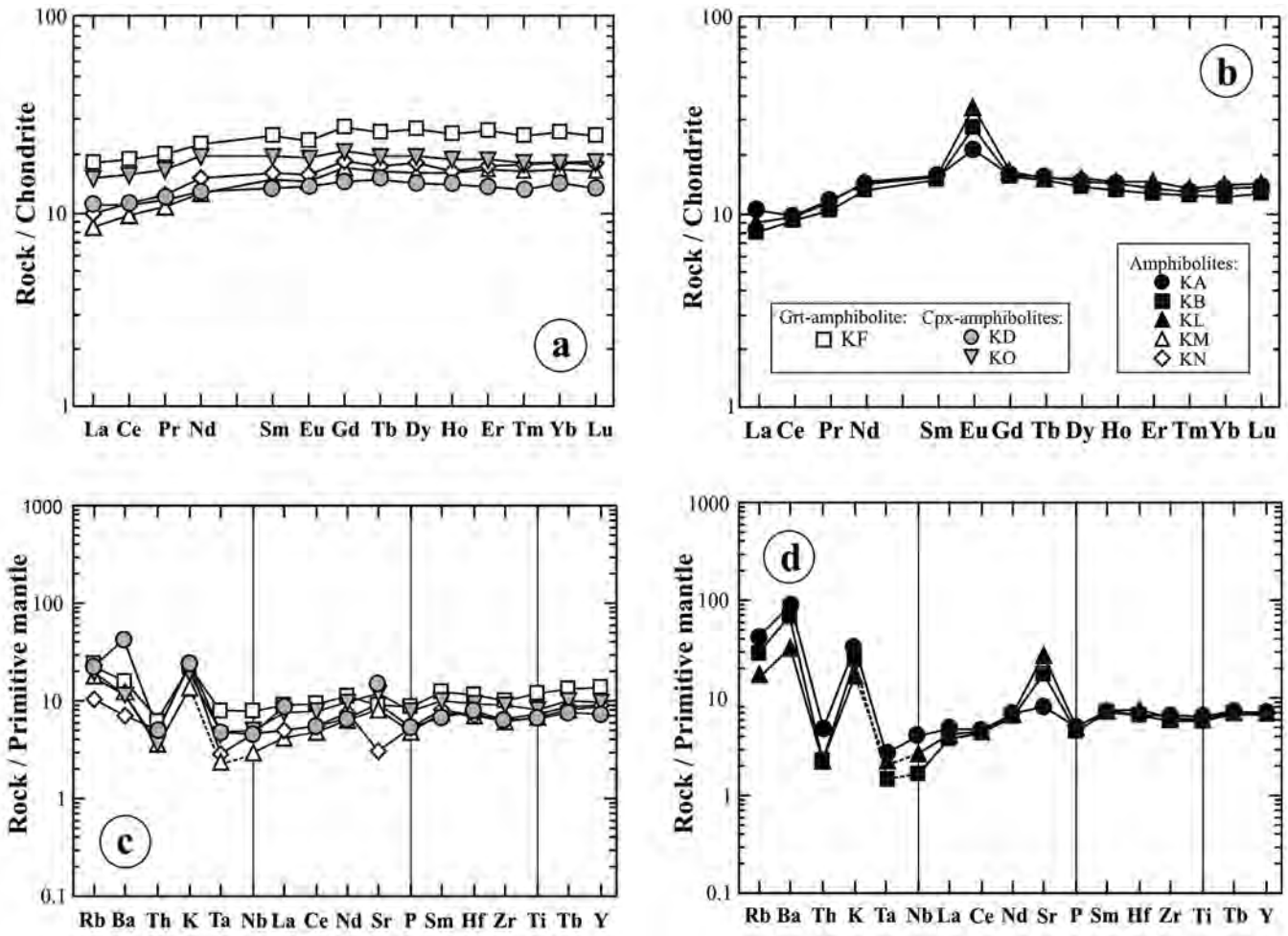


Fig. 8 - (a-b) REE-normalized patterns (McDonough and Sun, 1990) and (c-d) Primitive mantle normalized multi-element patterns (Hofmann, 1988) for amphibolites from the Kalnik Mt. metamorphic sole.

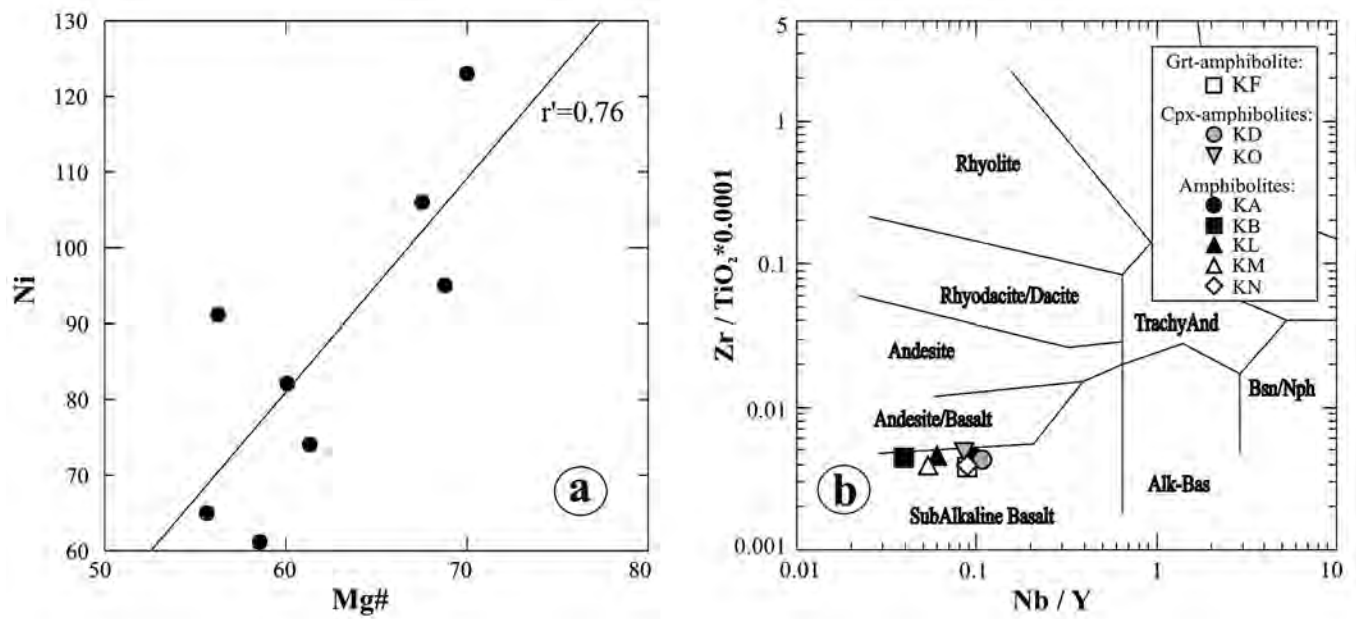


Fig. 9 - (a) Ni-Mg# variation diagram for amphibolites from the Kalnik Mt. metamorphic sole. (b) Classification diagram $Zr/TiO_2 \cdot 0.0001 - Nb/Y$ after Winchester and Floyd (1977) for amphibolites from the Kalnik Mt. metamorphic sole.

Table 5. Chemical composition of Kalnik Mt. amphibolites.

Sample Rock	KF	KD	KO	KA	KB	KL	KM	KN
	Grt-Am	Cpx-Am	Cpx-Am	Am	Am	Am	Am	Am
SiO ₂	43.56	48.40	48.49	45.57	45.95	46.09	45.53	43.82
TiO ₂	2.13	1.21	1.47	1.22	1.10	1.14	1.22	1.33
Al ₂ O ₃	13.24	14.26	14.67	14.81	14.53	15.49	14.15	13.62
FeO _{total}	16.66	10.32	11.79	10.79	9.60	10.04	11.60	12.79
MnO	0.47	0.18	0.20	0.20	0.19	0.19	0.20	0.23
MgO	7.72	7.95	5.47	5.65	5.64	5.59	9.45	11.05
CaO	8.69	10.65	10.08	11.56	13.35	14.77	11.51	10.89
Na ₂ O	2.73	3.05	3.94	2.50	2.57	1.90	2.21	2.05
K ₂ O	0.78	0.82	0.74	1.79	1.12	0.70	0.56	0.43
P ₂ O ₅	0.18	0.11	0.16	0.11	0.10	0.11	0.10	0.11
LOI	1.93	1.88	1.64	4.42	4.67	2.66	2.18	2.22
Total	98.09	98.83	98.65	98.62	98.82	98.68	98.71	98.54
Mg#	50.80	63.18	50.83	53.85	56.69	55.36	64.48	65.81
Cs	0.8	1.0	0.5	0.3	0.3	0.2	0.5	<0.1
Rb	13.0	11.4	10.3	24.9	16.0	10.1	9.7	5.6
Ba	94	249	71	598	440	209	75	43
Th	0.5	0.4	0.3	0.4	0.2	0.2	0.3	0.4
U	0.3	0.3	0.3	0.2	0.2	0.3	0.1	<0.1
Ta	0.3	0.2	0.2	0.1	<0.1	<0.1	<0.1	0.1
Nb	4.8	3.1	3.3	2.7	1.1	1.8	1.8	3.1
Pb	4.0	146.4	1.2	383.2	276.5	134.9	3.3	8.0
Sr	162	172	216	159	341	535	150	55
Zr	97	63	87	68	59	64	59	63
Hf	3.1	2.1	2.5	1.9	1.9	2.2	1.9	1.9
Y	54	29	39	29	28	30	34	35
Cr	68	212	96	281	260	274	205	239
Ni	65	106	91	61	74	82	95	123
Sc	53	42	44	43	39	42	45	50
Zn	86	104	47	376	233	239	30	90
V	488	283	303	260	248	276	340	361
La	5.6	3.4	4.7	3.2	2.5	2.8	2.6	3.1
Ce	15.1	8.9	12.6	7.9	7.4	7.8	7.8	9.0
Pr	2.44	1.42	2.05	1.42	1.27	1.39	1.32	1.51
Nd	13.4	7.7	11.6	8.6	8.0	8.8	7.5	9.0
Sm	4.8	2.6	3.8	3.0	2.9	3.0	2.9	3.1
Eu	1.73	1.00	1.40	1.56	2.01	2.59	1.06	1.14
Gd	7.08	3.77	5.31	4.05	4.02	4.29	4.42	4.72
Tb	1.23	0.70	0.93	0.73	0.70	0.72	0.77	0.82
Dy	8.62	4.56	6.26	4.68	4.39	4.83	5.13	5.74
Ho	1.82	1.00	1.35	1.03	0.94	1.05	1.14	1.18
Er	5.49	2.85	3.91	2.83	2.69	3.09	3.49	3.63
Tm	0.81	0.42	0.58	0.42	0.40	0.44	0.53	0.57
Yb	5.42	2.95	3.80	2.82	2.54	2.94	3.46	3.74
Lu	0.80	0.43	0.59	0.44	0.41	0.46	0.53	0.57

Mg# = $100 * \text{MgO} / (\text{MgO} + 0.8 * \text{FeO}_{\text{tot}})$. KF – garnet-amphibolite, KD and KO – clinopyroxene amphibolites, KA, KB, KL, KM, KN – common amphibolites.

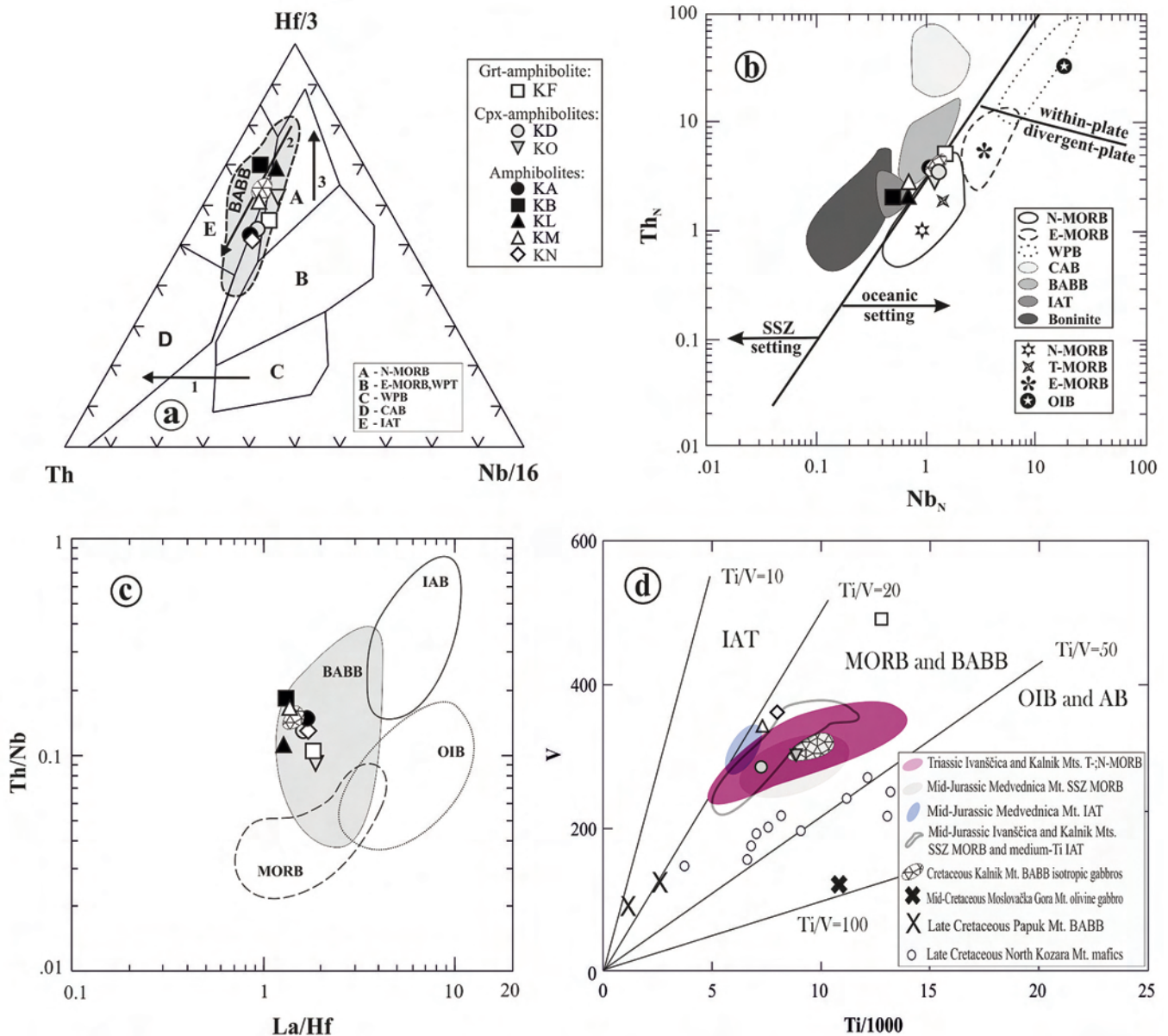


Fig. 10 - Discrimination diagrams for the amphibolites from the Kalnik Mt. metamorphic sole. (a) Th-Nb/16-Hf/3 diagram (Wood 1980). A- normal mid-ocean ridge basalts (N-MORB); B- enriched MORB (E-MORB) and within-plate tholeiites (WPT); C- alkaline within-plate basalts (AWPB); D- calc-alkaline basalts (CAB); E- island-arc tholeiites (IAT); 1- crustal contamination; 2- SSZ ophiolites trend; 3- MORB ophiolites trend. Data for back-arc basin basalts-BABB (shaded field) compiled from Saunders and Tarney (1979), Weaver et al. (1979), Crawford and Keays (1987), Jahn (1986), Leat et al. (2000). (b) Nb_N - Th_N diagram. Fields of different basaltic rock-type from the Albanide-Hellenide ophiolites are taken from Saccani et al. (2011). N-MORB, E-MORB and OIB are from Sun and McDonough (1989). T-MORB are from Geshi et al. (2007). (c) La/Hf-Th/Nb diagram (Paktunc 1990). (d) Ti/1000-V diagram (Shervais 1982). Data for field of Middle Jurassic Medvednica Mt. SSZ MORB and IAT effusives and dykes from Slovenec and Lugović (2009), for Middle Jurassic Ivanščica and Kalnik Mts. SSZ MORB and medium-Ti IAT effusives from Slovenec et al. (2011), for Cretaceous Kalnik Mt. BABB isotropic gabbros from Lugović et al. (2015), for Middle Cretaceous Moslavačka Gora Mt. olivine gabbro from Balen et al. (2003a), for Late Cretaceous Papuk Mt. BABB volcanites from Pamić et al. (2000) and for Late Cretaceous North Kozara Mt. mafics from Ustaszewski et al. (2009).

Metamorphic conditions

The retrograde processes which affected the metamorphic rocks of Kalnik Mt. caused albitization of plagioclase in most analysed samples, thus enabling the calculation of metamorphic temperatures based on amphibole - plagioclase equilibrium only in a limited number of samples (Table 6). On the other hand, the pressures conditions could be determined only for the garnet-bearing amphibolites. The peak metamorphic conditions were defined by the assemblage A (Hbl + Grt + Pl + Cpx), which corresponds to a temperature of $790 \pm 20^\circ\text{C}$ and pressures of 0.79 to 1.04 GPa. The pressure

estimates were made using both Mg and Fe calibrations and differences between the two are probably due to recalculations of Fe^{3+} in garnet and estimation of the andradite content (Kohn and Spear, 1990). Such peak values of metamorphic pressures and temperatures are in agreement with Na(M4) contents (0.4-0.6 a.p.f.u.) and Al^{IV}/Al^{VI} ratios (~ 2.70 - 4.24) of the amphiboles, which indicate pressures exceeding 0.5 GPa (Table 2, e.g., Raase et al., 1986). For the prograde assemblage C (Hbl + Pl + Ep + Cpx \pm Ttn \pm Kfs \pm Ap) of the clinopyroxene amphibolites lower temperatures were estimated ($660 \pm 50^\circ\text{C}$). Yet, these might have been slightly underestimated considering that the appearance of clinopyroxene in

Table 6. Results of geothermobarometric calculations for amphibolites from the Kalnik Mt. amphibolites.

Sample	Kohn & Spear p (GPa)	Holland & Blundy T (°C)
KB	x	x
KD	x	660±40
KF	0.79 (Mg) – 1.04 (Fe)	790±20
KM	x	x
KN	x	x
KO	x	660±50

KF – garnet-clinopyroxene amphibolite, KD and KO – clinopyroxene amphibolites, KB, KN, KM – common amphibolites. x – pressures and temperatures impossible to calculate due to the lack of garnet or complete alteration of plagioclase, respectively.

Opx-free metabasic systems requires a minimum temperature of about 700°C (Guilmette et al., 2008). The peak metamorphic conditions for the assemblage A are further corroborated by the lack of metamorphic epidote in the first type of amphibolite (assemblage A), suggesting its complete consumption by the prograde metamorphism, whereas in the second type of amphibolite (assemblage C) epidote is still preserved. Finally, the experimental studies on natural, low-K, calcic amphibolites showed that at about 1.0 GPa and 750 to 1000°C garnet first appears at 850°C (Wolf and Wyllie, 1994), which is consistent with the estimated peak conditions. Despite the difficulties in P-T calculations caused by retrograde processes, evidence for a prograde metamorphic evolution for *garnet-* and *clinopyroxene amphibolite* is thus provided. For the clinopyroxene amphibolite, the prograde trend is well traced by the “U”-shaped deployment of the pistacite component in epidote and by the appearance of clinopyroxene. The garnet amphibolite represents a peak metamorphic assemblage defined by the formation of garnet porphyroblasts following the reaction of amphibole and plagioclase, as well as the disappearance of epidote. Although for *common amphibolites* it was not possible to determine metamorphic conditions due to plagioclase albitization, they may have been characterized by lower values of peak metamorphism insufficient to initiate amphibole dehydration to form clinopyroxene and An-rich plagioclase at around 750-800°C (e.g., Bucher and Frey, 1994).

The retrograde evolution of the amphibolites is documented by garnet decomposition and widespread formation of low-grade hydrous minerals. The origin of garnet kelyphitic rims is usually explained by retrograde metamorphism under decreasing pressure conditions, which led to garnet breakdown and formation of hydrous secondary species (e.g., Prakash et al., 2007). The appearance of “metamorphic vermiculite”, an intimately interlayered 10-Å mica and Fe-rich 14-Å chlorite, was also documented in the garnet kelyphitic coronas. This testifies garnet instability at low-grade metamorphic conditions taking into account that this mineral forms at $T < 500^{\circ}\text{C}$ and low pressures (0.2-0.4 GPa) (Ruiz Cruz, 2003). Most common retrograde phases in the amphibolites include acicular actinolite, muscovite, chlorite, and albitic plagioclase. Fe-pumpellyite and prehnite also replace plagioclase, whereas secondary amphibole (tremolite-actinolite), chlorite, and clinozoisite form at the expense of primary amphibole and epidote. Calcite with minor clinozoisite, prehnite and albite is found as infill of

veins and fractures. The clinozoisite-pumpellyite-tremolite/actinolite-albite-chlorite mineral associations indicate retrograde P-T conditions of around 0.2-0.6 GPa at 300-400°C (Parkinson, 1998). The retrograde re-equilibration was linked to exhumation and metamorphic rock emplacement, which led to a greenschist to sub-greenschist facies overprint.

Nature of metamorphism and regional geodynamic significance of Kalnik Mt. amphibolites

Geochemistry of the analysed metabasites allows to recognize high-Ti BABB tholeiitic extrusives and low-Ti IAT-like cumulates as the most plausible protoliths of Kalnik Mt. amphibolites (Figs. 8, 10). Such igneous precursors are linked to mantle-derived basaltic melts formed at a back-arc spreading centre as suggested by HFS elements depletion, which are typical features of supra-subduction-related (SSZ) igneous rocks (Gill, 2010). The composite affinity of SSZ-related igneous protolith of the Kalnik Mt. amphibolites (i.e. extrusives vs. cumulates) supports an origin in a initial intra-oceanic subduction setting of a back-arc oceanic environment (e.g., Lázaro et al., 2013). The occurrence of such composite mafic series consisting of both cumulate and extrusive igneous rocks is encountered in many ophiolite complexes where a metamorphic sole is documented, e.g., Dinarides (Bosnia), Pamić et al., 2002; Albanides (Albania), Gaggero et al., 2009; Semail (Oman), Godard et al., 2006; Eldivan (Turkey), Dangerfield et al., 2011. Tectonic juxtaposition of different oceanic segments brought together during the ophiolite obduction and emplacement is usually considered responsible for such a tectonic mixing of distant bodies of BABB oceanic crust (Lázaro et al., 2013).

In an attempt to identify the protolith(s) of Kalnik Mt. amphibolites and to put them and their metamorphic derivatives in the geotectonic frame of Tethyan Mesozoic development, we compared the geochemistry of Triassic and Jurassic mafic rocks scattered throughout the Sava Unit (Fig. 1; e.g., Slovenec and Lugović, 2008; 2009; Slovenec et al., 2010) with the composition of the amphibolites of this study (Figs. 10d, 11). Additionally, the basaltic igneous rocks of the Kozara Mt. (North of Bosnia and Herzegovina), thought to have been generated in a Cretaceous marginal basin (Fig. 1), were also taken into account as potential protoliths. The normalized values of REE concentrations in the

Kalnik Mt. amphibolites compared with its counterparts from a set of potential magmatic protoliths indicate the Middle Jurassic SSZ ophiolitic rocks of the Sava Unit as the most likely precursor rocks (Fig. 11).

Despite a lack of general consensus on the geotectonic affinity of mafic rocks from the studied area (Dinaric vs. Meliata-Maliac), tectono-magmatic evolution of the crust formed in different oceanic settings is well documented (Slovenec and Lugović, 2008; 2009; Slovenec et al., 2010; 2011; Kiss et al., 2012; Lugović et al., 2015). The oceanic crust started to form at a spreading ridge in Ladinian time (Fig. 12a), following an earlier continental rifting, and lasted until the Middle Jurassic (Bajocian; Fig. 12a). The initiation and onset of intraoceanic subduction commenced thereupon in the Bathonian time, recorded by subduction of an active oceanic ridge crust (Fig. 12b). Such a regime with new-born infant proto-arc prograded toward the creation of a back-arc basin in upper Middle to mid Late Jurassic (Callovian - Kimmeridgian), possibly as a result of slab roll-back (Fig. 12b-c). Widespread high-Ti BABB and MOR extrusives and low-Ti IAT lavas and composite fragments of SSZ upper crust, both likely to be precursors of studied amphibolites, characterize this step of geodynamic evolution of nowadays Sava Unit igneous suites. The biggest portion of the crust was consumed during the final closure of Dinaric Tethys at the Late Jurassic (Fig. 12d), whilst only remnants of ancient crust have been preserved as slices and blocks in the ophiolite mélangé formed in an accretionary wedge that was obducted onto the northern passive margins of Adria at the onset of the Cretaceous (e.g., Festa et al., 2010; Fig. 12e).

Taking into account the field relationships, geochemical similarities, and petrology of their igneous protoliths, the Kalnik Mt. amphibolites can be considered as a *metamorphic sole* originated in a nascent subduction/obduction system formed in response to the onset of convergent processes near a back-arc oceanic spreading axis where the oceanic lithosphere was still hot (Bortolotti et al., 2002; Robertson, 2004; Dewey and Casey, 2011; Saccani et al., 2011). In the

model we propose (Figs. 12b-c), the Middle Jurassic high- and low-Ti mafic rocks that evolved in a BAB spreading ridge, were affected by the pre-Tithonian subduction initiation in a way that closely corresponds to the models developed for Oman ophiolites (e.g., Boudier et al., 1985; 1988). Belonging to the oceanic crust of the lower plate these mafic rocks re-crystallized when overthrust by young and hot oceanic lithosphere (Fig. 12c, enlarged detail). As reported for many Tethyan ophiolites this metamorphic sole was henceforth detached from the down-going plate (Fig. 12c, enlarged detail) and finally thrust on the Adria margin (Fig. 12d-e) within the next 10-15 Ma (i.e. until Early Cretaceous, Pamić et al., 2002; Balen et al., 2003a; 2003b; Bortolotti et al., 2005). The estimated peak temperature conditions (700-800°C) are within the typical range suggested for the metamorphic sole, whilst the estimated pressures of approximately 0.8 to 0.9 GPa suggest that magmatic protoliths have never been dragged at great depth (> 30 km at geostatic gradient of 35 km/GPa). Still, the thickness of peridotite blocks in the Kalnik Mt. ophiolite mélangé does not support such pressures (Šimunić et al., 1981). This apparent disproportion in pressure poses a known problem in the explanation of the sole rock genesis and several explanatory models have so far been proposed (e.g., Robertson, 2004). The widely accepted model of Hacker and Gnos (1997) and Casey and Dewey (1984) advocate the thinning of a mantle section during the intraoceanic subduction, which may lead to the extensional collapse of the overlying ophiolite once the deeper subduction levels are reached. Metamorphic pressures are, however, consistent with the development of a new supra-subduction environment in the pre-existing spreading centre(s) of back-arc setting (Fig. 12c, enlarged detail). Furthermore, the proposed prograde metamorphic evolution of the Kalnik Mt. metamorphic sole well approaches the category of “high-temperature” soles (600-750°C and 0.9-1.1 GPa) of Flower and Dilek (2003) and is compatible with the model of Peacock et al., (1994) which describes metamorphism of young subducted oceanic crust under hot mantle at a constant shear.

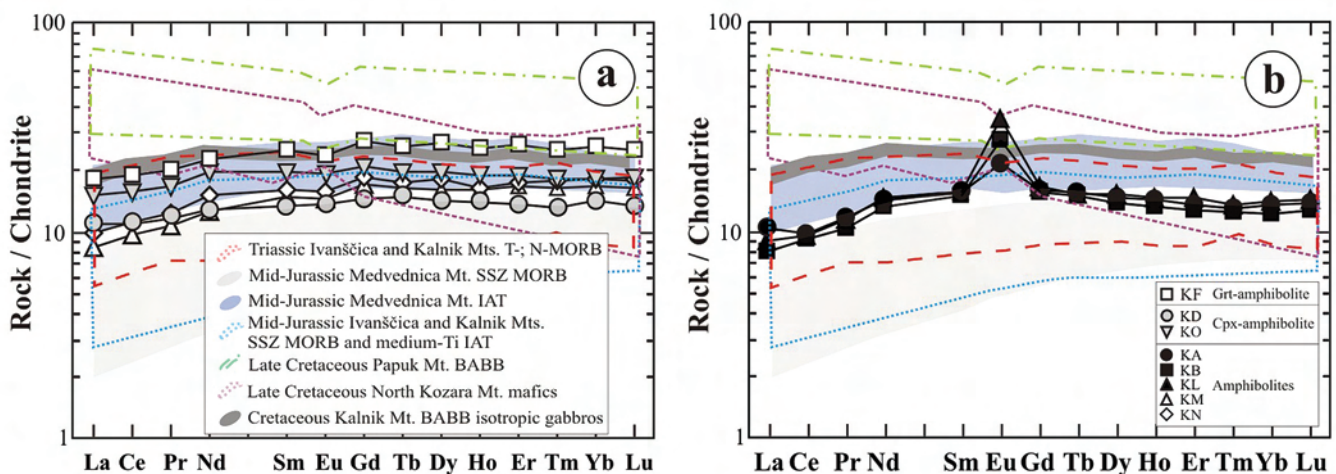


Fig. 11 - (a) and (b) Chondrite-normalized REE patterns (McDonough and Sun, 1990) for Middle Jurassic Medvednica Mt. SSZ MORB and IAT effusives and dykes (Slovenec and Lugović, 2009), Middle Jurassic Ivanščica and Kalnik Mts. SSZ MORB and IAT (Slovenec et al., 2011), Late Cretaceous Papuk Mt. BABB volcanics (Pamić et al., 2000), Late Cretaceous North Kozara Mt. Mafic rocks (Ustaszewski et al., 2009) and Cretaceous Kalnik Mt. gabbros (Lugović et al., 2015).

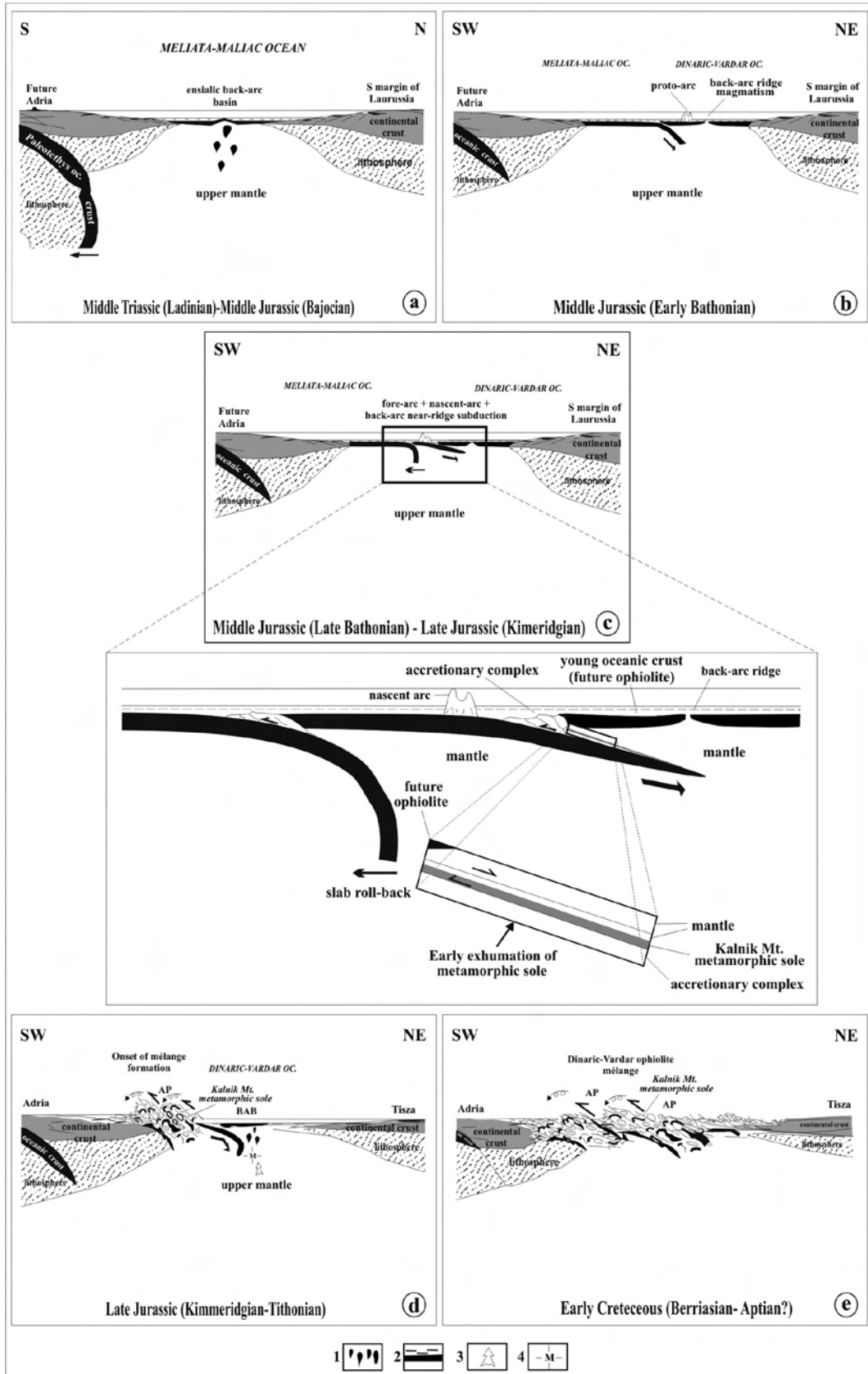


Fig. 12 - Rough schematic geodynamic evolutionary model for the north-western branch of Dinaric-Vardar Tethys (not to scale). (a) The spreading stage. (b) The early stage of the subduction with formation of an infant proto-arc and ridge in the ensialic marginal (back-arc) basin. (c) The back-arc near-ridge subduction stage. Sketch detail: initiation of intra-oceanic subduction and formation of metamorphic sole and subsequent early exhumation of metamorphic sole relative to the ophiolite (adapted after Wakabayashi and Dilek, 2003). (d) The evolved subduction stage and progressive accretionary emplacement. (e) The ophiolite obduction and final stage of oceanic closure.

As mentioned above, a maximum time span of ~ 20 Ma can be constrained between the initial subduction of mid-Jurassic mafic suites in the back-arc setting that gave rise to the formation of studied amphibolites and their final emplacement/obduction as a part of ophiolitic mélange on top of the Adria passive margins during Tithonian to Berriasian (Fig. 12c-e). The entire process of subduction initiation in a back-arc setting, proto fore-arc development, initial subduction, and crust-continent collision likely took place in a very short time. According to Dewey and Casey (2011) the thermal thickening of the fore-back-arc system is maintained by its position above the down-going oceanic crust and if obduction onto a continental margin is to occur, it must take place within 10-15 million years, which is in good agreement with our reconstruction of the Kalnik Mt. amphibolite evolution. Otherwise, if the age of upper ophiolite plate would have exceeded significantly 20 Ma, the lithosphere becomes too thick to obduct, bulldozing the continental margin it collides with.

An alternative to the proposed petrogenetic model for the Kalnik Mt. amphibolites is regional (Barrovian) metamorphism, which took place at the time of collision and subsequent obduction of an infant oceanic arc and related supra-subduction ophiolites of the Dinaric Neotethys on the passive margins of Adria microplate in Late Jurassic-Early Cretaceous (Belak et al., 1995). The ortho-greenschists of the neighbouring Medvednica Mt. (Figs. 1-2) are thought to have originated following this mechanism (Lugović et al., 2006). Still, ascribing the origin of the investigated amphibolites to the regional metamorphism and ophiolite obduction raise several issues. First, the collisional regional metamorphism would require a substantial crustal thickening and deformation of the continental margin structural pile, which is difficult to reconcile with the field relations of the NW Adria margins (Pinter et al., 2006; Handy et al., 2010). Even if the episodic orogenesis did occur it lasted relatively shortly, assuming it coincided with the Oxfordian to Berriasian ophiolite obduction (Belak et al., 1995), which is inconsistent with the conductive heat transfer in over-thickened crust seen as a thermal cause of metamorphism (e.g., England and Thompson, 1984). Moreover, no syn-orogenic intrusive rocks that could have served as heat source are reported in the Sava Unit (Pamić, 1997b). If the origin of the amphibolites is to be linked to the obduction of hot ophiolite slab only, some additional concerns may come forth. The estimated metamorphic pressures for instance (0.8 to 0.9 GPa, Table 6) are not attainable, whilst the recent one-dimensional heat modelling made for the obduction of 900°C, 10-km-thick oceanic lithosphere onto a cold continental margin (200°C) predicts temperatures greater than 400°C only in the upper 2 km of the footwall (Chew et al., 2010). However, this is at variance with the peak metamorphic temperatures obtained for the Kalnik Mt. amphibolites (700-800°C, Table 6). Such mechanism rather explains the metamorphism of passive margin sediments under medium- to low-grade conditions during obduction of the ophiolitic napes as reported in many Tethyan ophiolites (e.g., Cluzel et al., 2012).

Assessing the above mentioned geotectonic scenarios and bearing in mind that most of the field information on analysed amphibolites was derived from an ophiolite mélange where it is very difficult to reconstruct the original relations between the units, we propose the Kalnik Mt. amphibolites formed as a metamorphic sole in the Middle to Late Jurassic back-arc basin of Dinaric Tethys at the onset of subduction/thrusting processes. Late Jurassic and Early

Cretaceous obduction of Dinaric ophiolites may have also transported parts of the metamorphic sole rocks onto the NW margins of Adria microplate incorporating them in present-day ophiolite mélange of Sava Unit.

CONCLUSIONS

Nemato- to granoblastic lenses of fine-grained amphibolites outcrop in hectometre-sized blocks in the ophiolite mélange of the Kalnik Mt. in northwest Croatia. Based on petrological and geochemical evidences we infer that these rocks present relics of a metamorphic sole formed in an incipient subduction zone of the back-arc basin of northern segment of Dinaric Tethys. The age of the igneous protoliths suggest that the metamorphic event most likely occurred in Upper Jurassic pre-Tithonian time. The back-arc supra-subduction setting was short-living (~ 20 Ma), lasting until the final obduction of ophiolites, including the sole amphibolites, onto the northern passive margins of Adria in Late Jurassic and Early Cretaceous, as suggested by geological evidences. Based on metamorphic paragenesis, three types of amphibolites were recognized: (b) garnet amphibolite, (b) clinopyroxene amphibolite and (c) common amphibolite. Using conventional thermobarometers for mafic rocks, peak metamorphic conditions were estimated to have reached approximately 800°C and 0.8 to 0.9 GPa, whilst the retrograde mineral assemblages correspond to greenschist to sub-greenschist facies conditions. Immobile trace element geochemistry indicate back-arc ridge tholeiitic extrusives and island arc tholeiitic cumulates as igneous protoliths of the amphibolites. This study provides the first detailed piece of evidence for the occurrence of metamorphic sole rocks in Sava Unit of NW Dinarides. It also provides additional constraints on the Late Jurassic - Early Cretaceous Neotethyan geodynamics marked by the subduction in a back-arc basin and penecontemporaneous ophiolite emplacement.

ACKNOWLEDGMENTS

The present study is the result of the scientific projects "Tectonomagmatic correlation of fragmented oceanic lithosphere in the Dinarides" (grant No. 195-1951126-3205 to B.L.) and "Mesozoic magmatic, mantle and pyroclastic rocks of north-western Croatia" (grant no. 181-1951126-1141 to Da. S.) carried out under the support of the Croatian Ministry of Science, Education and Sports. We thank Ilona Finn (University of Heidelberg/Germany) for providing us with excellent thin sections. A. Ristić and Z. Peh are thanked for his help with English. Critical comments by S. Schmid and D. Milovanović greatly helped to improve an early version of the manuscript. Finally, constructive reviews by A. Montanini and one anonymous reviewer, as well as the editorial handling and suggestions by L. Pandolfi contributed significantly to the manuscript quality.

REFERENCES

- Arnason J.G., Bird D.K. and Liou J.G., 1993. Variables controlling epidote composition in hydrothermal and low-pressure regional metamorphic rocks. *Abh. Geol. B.-A.*, 49: 17-25.
- Babić L. and Zupanić J., 2002. The Jurassic ophiolitic mélange in the NE Dinarides: Dating, internal structure and geotectonic implications. *Ecl. Geol. Helv.*, 95: 263-275.

- Balen D., Schuster R., Garašić V. and Majer V., 2003a. The Kremenjača olivine gabbro from Moslavačka Gora (South Tisia, Croatia). *Rad Hrvatske Akad. znanosti i umjetnosti. Prirodne znanosti*, 486: 57-76.
- Balen D., Opereta M. and Pamić J., 2003b. The geothermobarometry of Alpine amphibolites from the metamorphic sole of Krivaja-Konjuh ultramafic massif (Dinaride ophiolite zone, Bosnia). In: L. Csontos (Ed.), *Proceed. 6th Alpine Workshop 35*, Sopron, Hungary. *Ann. Univ. Sci. Budapest. Sect. Geol.*, p. 131-132.
- Bébian J., Dimo-Lahitte A., Vergély P., Insergueix-Filippi D. and Dupeyrat L., 2000. Albanian ophiolites. I - magmatic and metamorphic processes associated with the initiation of a subduction. *Ofioliti*, 25: 39-45.
- Beccaluva L., Piccardo G.B. and Serri G., 1980. Petrology of Northern Apennine ophiolites and comparison with other Tethyan ophiolites. In: A. Panayiotou (Ed.), *Proceed. Intern. Ophiolite Conf.*, Nicosia, Cyprus, p. 314-331.
- Belak M., Pamić J., Kolar-Jurkovšek T., Pescaskay Z. and Karan D., 1995. Alpinski regionalnometamorfni kompleks Medvednice (sjeverozapadna Hrvatska) In: I. Vlahović, I. Velić and M. Šparica (Eds.), *Proceed. 1st Croatian Geol. Congr.*, Opatija, Croatia, p. 67-70. (in Croatian).
- Beiersdorf R.E. and Day H.W., 1995. Mineral paragenesis of pumpellyite in low-grade mafic rocks. In: P. Schifman and H.W. Day (Eds.), *Low grade metamorphism of mafic rocks*. *Geol. Soc. Am. Spec. Pap.*, 296: 5-27.
- Bortolotti V., Marroni M., Pandolfi L. and Principi G., 2005. Mesozoic to Tertiary tectonic history of the Mirdita ophiolites, northern Albania. *Island Arc*, 14: 471-493.
- Bortolotti V., Marroni M., Pandolfi L., Principi G. and Saccani E., 2002. Interaction between mid-ocean ridge and subduction magmatism in Albanian ophiolites. *J. Geol.*, 110: 561-576.
- Bortolotti V., Chiari M., Marroni M., Pandolfi L., Principi G. and Saccani E., 2013. The geodynamic evolution of the ophiolites from Albania and Greece, Dinaric-Hellenic Belt: one, two, or more oceanic basins? *Int. J. Earth Sci.*, 102: 783-811. DOI: 10.1007/s00531-012-0835-7.
- Boudier F., Bouchez J.L., Nicolas A., Cannat M., Ceuleneer G., Misseri M. and Montigny R., 1985. Kinematics of oceanic thrusting in the Oman ophiolite: model of plate convergence. *Earth Planet. Sci. Lett.*, 75: 215-222.
- Boudier F., Ceuleneer G. and Nicolas A., 1988. Shear zones, thrusts and related magmatism in the Oman ophiolite: Initiation of thrusting on an oceanic ridge. *Tectonophysics*, 151: 275-296.
- Bucher K. and Frey M., 1994. *Petrogenesis of metamorphic rocks*. Springer, Berlin, 500 pp.
- Burke K., 2011. Plate tectonics, the Wilson Cycle, and mantle plumes: Geodynamics from the top. In: R. Jeanloz and K.H. Freeman (Eds.), *Ann. Rev. Earth Planet. Sci.*, 39: 1-29.
- Casey J.F. and Dewey J.F., 1984. Initiation of subduction zones along transform and accreting plate boundaries, triple-junction evolution, and forearc spreading centres - implications for ophiolitic geology and obduction. *Geol. Soc. London Spec. Publ.*, 13: 269-290.
- Cavazza W., Roure F., Spakman W., Stampfli G.M. and Ziegler P.A., 2004. *The TRANSMED Atlas - The Mediterranean region from Crust to Mantle*. Springer, Berlin Heidelberg, 141 pp.
- Chen C.-Y., Frey F.A. and Garcia M.O., 1990. Evolution of alkalic lavas at Haleakala Volcano, east Maui, Hawaii. *Contrib. Mineral. Petrol.*, 105: 197-218.
- Chew D.M., Daly J.S., Magna T., Page L.M., Kirkland C.L., Whitehouse M.J. and Lam R., 2010. Timing of ophiolite obduction in the Grampian orogeny. *Geol. Soc. Am. Bull.*, 122: 1787-1799.
- Clague D.A. and Frey F.A., 1982. Petrology and trace element geochemistry of the Honolulu Volcanism, Oahu: implications for the oceanic mantle below Hawaii. *J. Petrol.*, 23: 447-504.
- Cluzel D., Jourdan F., Meffre S., Maurizot P. and Lesimple S., 2012. The metamorphic sole of New Caledonia ophiolite: ⁴⁰Ar/³⁹Ar, U-Pb, and geochemical evidence for subduction inception at a spreading ridge. *Tectonics*, 31, TC 3016.
- Crawford A.J. and Keays R.R., 1987. Petrogenesis of Victorian Cambrian tholeiites and implications for the origin of associated boninites. *J. Petrol.*, 28: 1075-1109.
- Dangerfield A., Harris R., Sarifakioğlu E. and Dilek Y., 2011. Tectonic evolution of the Ankara Mélange and associated Eldivan ophiolite near Hançili, central Turkey. *Geol. Soc. Am. S.*, 480: 143-169.
- Deer W.A., Howie R.A. and Zussman J., 1996. *An Introduction to the rock-forming minerals*, 2nd ed., Prentice Hall, Harlow, Essex, England; New York, NY, 712 pp.
- Dewey J.F. and Casey J.F., 2011. The origin of obducted large-slab ophiolite complexes. In: *Arc-continent collision, Frontiers in Earth Sciences*. Springer, Berlin Heidelberg, p. 431-444.
- Dilek Y. and Whitney D.L., 1997. Counter clockwise P-T-t trajectory from the metamorphic sole of a Neo-Tethyan ophiolite (Turkey). *Tectonophysics*, 280: 295-310.
- England P.C. and Thompson A.B., 1984. Pressure-temperature-time paths of regional metamorphism I. Heat transfer during the evolution of regions of thickened continental crust. *J. Petrol.*, 25: 894-928.
- Festa A., Pini G.A., Dilek Y. and Codegone G., 2010. Mélanges and mélange-forming processes: a historical overview and new concepts. *Int. Geol. Rev.*, 52: 1040-1105.
- Flower M.F.J. and Dilek Y., 2003. Arc-trench rollback and forearc accretion: 1. A collision-induced mantle flow model for Tethyan ophiolites. *Geol. Soc London Spec. Publ.*, 218: 21-41.
- Gaggero L., Marroni M., Pandolfi L. and Buzzi L., 2009. Modeling the oceanic lithosphere obduction: Constraints from the metamorphic sole of Mirdita ophiolites (northern Albania). *Ofioliti*, 34: 17-42.
- Geshi N., Umino S., Kumagai H., Sinton J.M., White S.M., Kishimoto K. and Hilde T.W., 2007. Discrete plumbing systems and heterogeneous magma sources of a 24 km³ off-axis lava field on the western flank of East Pacific Rise, 14° S. *Earth Planet. Sci. Lett.*, 258: 61-72.
- Gill R., 2010. *Igneous rocks and processes: A practical guide*. Wiley-Blackwell, Chichester, 440 pp.
- Gjata K., Kornprobst J., Kodra A., Briot D. and Pineau F., 1992. Subduction chaude à l'aplomb d'une dorsale? Exemple des enclaves de pyroxénite à grenat de la brèche serpentineuse de Derveni (Albanie). *Boll. Soc. Géol. Fr.*, 163: 469-476.
- Godard M., Bosch D. and Einaudi F., 2006. A MORB source for low-Ti magmatism in the Semail ophiolite. *Chem. Geol.*, 234: 58-78.
- Gottlieb P., Wilkie G., Sutherland D., Ho-Tun E., Suthers S., Perera K., Jenkins B., Spencer S., Butche A. and Rayner J., 2000. Using quantitative electron microscopy for process mineralogy applications. *J.O.M.*, 52: 24-25.
- Grapes R.H. and Graham C.M., 1978. The actinolite-hornblende series in metabasites and the so-called miscibility gap: A review. *Lithos*, 11: 85-92.
- Greenfield J.E., Clarke G.L. and White R.W., 1998. A sequence of partial melting reactions at Mt. Stafford, central Australia. *J. Metamorph. Geol.*, 16: 363-378.
- Guilmette C., Hébert R., Dupuis C., Wang C. and Li Z., 2008. Metamorphic history and geodynamic significance of high-grade metabasites from the ophiolitic mélange beneath the Yarlung Zangbo ophiolites, Xigaze area, Tibet. *J. Asian Earth Sci.*, 32: 423-437.
- Haas J., Mioč P., Pamić J., Tomljenović B., Árkai P., Bérczi-Makk A., Koroknai B., Kovács S. and Rálich-Felgenhauer E., 2000. Complex structural pattern of the Alpine-Dinaridic-Pannonian triple junction. *Int. J. Earth Sci.*, 89: 377-389.
- Hacker B.R. and Gnos E., 1997. The conundrum of Semail: explaining the metamorphic history. *Tectonophysics*, 279: 215-226.
- Halamić J., 1998. *Litostratigrafska karakterizacija jurskih i krednih sedimenata s ofiolitima Medvednice, Kalnika i Ivanšćice*. Ph.D. thesis, Univ. Zagreb, Zagreb, Croatia, 188 pp. (in Croatian).
- Halamić J., Marchig V. and Goričan Š., 1999. Geochemistry of Triassic radiolarian cherts in north-western Croatia. *Geol. Carpath.*, 52: 327-342.

- Handy M.R., Schmid S.M., Bousquet R., Kissling E. and Bernoulli D., 2010. Reconciling plate-tectonic reconstructions of Alpine Tethys with the geological-geophysical record of spreading and subduction in the Alps. *Earth Sci. Rev.*, 102: 121-158.
- Harlov D., Tropper P., Seifert W., Nijland T. and Förster H.-J., 2006. Formation of Al-rich titanite (CaTiSiO₄O-CaAlSiO₄OH) reaction rims on ilmenite in metamorphic rocks as a function of fH₂O and fO₂. *Lithos*, 88: 72-84.
- Hey M.H., 1954. A new review of chlorites. *Mineral. Mag.*, 224: 277-292.
- Higgins J.B. and Ribbe P.H., 1976. The crystal chemistry and space groups of natural and synthetic titanites. *Am. Mineral.*, 61: 878-888.
- Hofmann A.W., 1988. Chemical differentiation of the Earth: the relationship between mantle, continental crust, and oceanic crust. *Earth Planet. Sci. Lett.*, 90: 297-314.
- Holland T. and Blundy J., 1994. Non-ideal interactions in calcic amphiboles and their bearing on amphibole-plagioclase thermometry. *Contr. Mineral. Petrol.*, 116: 433-447.
- Jahn B., 1986. Mid-ocean ridge or marginal basin origin of the East Taiwan Ophiolite: chemical and isotopic evidence. *Contrib. Mineral. Petrol.*, 92: 194-206.
- Jappy T.G., Leake B.E. and Fallick A.E., 2001. Relationships between hornblende K-Ar ages, chemical composition and hydrogen isotopes, Connemara, western Ireland: evidence for a massive extinct hydrothermal system. *J. Geol. Soc.*, 158: 843-854.
- Kiss G., Molnár F., Palinkaš L.A., Kovács S. and Hrvatović H., 2011. Correlation of Triassic advanced rifting-related Neotethyan submarine basaltic volcanism of the Darnó Unit (NE-Hungary) with some Dinaridic and Hellenidic occurrences on the basis of volcanological, fluid-rock interaction, and geochemical characteristics. *Int. J. Earth Sci.*, 101: 1503-1521.
- Kohn M.J. and Spear F.S., 1990. Two new geobarometers for garnet amphibolites, with applications to southeastern Vermont. *Am. Mineral.*, 75: 89-96.
- Lanphere M., Coleman R.C., Karamata S. and Pamić J., 1975. Age of amphibolites associated with Alpine peridotites in the Central Dinaride Ophiolite Belt, Yugoslavia. *Earth Planet. Sci. Lett.*, 26: 271-276.
- Lázaro C., Blanco-Quintero I.F., Rojas-Agramonte Y., Proenza, J.A., Núñez-Cambra K. and García-Casco A., 2013. First description of a metamorphic sole related to ophiolite obduction in the northern Caribbean: Geochemistry and petrology of the Güira de Jauco Amphibolite complex (eastern Cuba) and tectonic implications. *Lithos*, 179: 193-210.
- Leake B.E., Woolley A.R., Arps C.E.S., Birch W.D., Gilbert M.C., Grice J.D., Hawthorne F.C., Kato A., Kisch H.J., Krivovichev V.G., Linthout K., Laird J., Mandarino J.A., Maresch W.V., Nickel E.H., Rock N.M.S., Schumacher J.C., Smith D.C., Stephenson N.C.N., Ungaretti L., Whittaker E.J.W. and Youzhi, G., 1997. Nomenclature of amphiboles: Report of the Subcommittee on Amphiboles of the International Mineralogical Association, Commission on New Minerals and Mineral Names. *Am. Mineral.*, 82: 1019-1037.
- Leat P.T., Livermore R.A., Millar I.L. and Pearce J.A., 2000. Magma supply in back-arc spreading centre Segment E2, East Scotia Ridge. *J. Petrol.*, 41: 845-866.
- Liou J.G., Maruyama S. and Cho M., 1985. Phase equilibria and mineral parageneses of metabasites in low grade metamorphism. *Mineral. Mag.*, 49: 321-333.
- Lugović B., Šegvić B. and Altherr R., 2006. Petrology and tectonic significance of greenschists from the Medvednica Mts. (Sava Unit, NW Croatia). *Ofioliti*, 31: 39-50.
- Lugović B., Slovenec D., Halamić J. and Altherr R., 2007. Petrology, geochemistry and tectonic significance of Mesozoic ultramafic rocks from the Zagorje-Mid-Transdanubian Zone in Croatia. *Geol. Carpath.*, 58: 511-530.
- Lugović B., Slovenec D., Schuster R., Schwarz W.H. and Horvat M., 2015. Petrology, geochemistry and tectono-magmatic affinity of gabbroic olistoliths from the ophiolite mélange in the NW Dinaric-Vardar ophiolite zone (Mts. Kalnik and Ivanščica, North Croatia). *Geol. Croat.*, 68: 25-49.
- Mahoney J.J., Sinton J.M., Kurz M.D., Macdougall J.D., Spencer K.J. and Lugmair G.W., 1994. Isotope and trace element characteristics of a super-fast spreading ridge: East Pacific rise, 13-23°S. *Earth Planet. Sci. Lett.*, 121: 173-193.
- McDonough W.F. and Sun S.S., 1990. Composition of the Earth's primitive mantle. In: B.R. Lipin and G.A. McKay (Eds.), *Geochemistry and mineralogy of REE*. *Rev. Mineral.*, 21: 99-145.
- Morimoto N., 1988. Nomenclature of pyroxenes. *Miner. Petrol.*, 39: 55-76.
- Mukhopadhyay B., 1991. Garnet-clinopyroxene geobarometry: the problems, a prospect, and an approximate solution with some applications. *Am. Mineral.*, 76: 512-529.
- Operta M., Pamić J., Balen D. and Tropper P., 2003. Corundum-bearing amphibolites from the metamorphic basement of the Krivaja-Konjuh ultramafic massif (Dinaride Ophiolite Zone, Bosnia). *Mineral. Petrol.*, 77: 287-295.
- Paktunc A.D., 1990. Geochemical constraints on the tectonic setting of the mafic rocks of the Bathurst Camp, Appalachian Orogeny. *Can. J. Earth Sci.*, 27: 1182-1193.
- Pamić J., 1997a. The north-westernmost outcrops of the Dinaridic ophiolites: a case study of Mt. Kalnik (North Croatia). *Acta Geol. Hung.*, 40: 37-56.
- Pamić J., 1997b. Volcanic rocks of the Sava-Drava interfluvium and Baranja (in Croatian with English summary). *Nafta*, 8, 192 pp.
- Pamić J. and Tomljenović B., 1998. Basic geologic data from the Croatian part of the Zagorje-Mid-Transdanubian Zone. *Acta Geol. Hung.*, 41: 389-400.
- Pamić J., Gušić I. and Jelaska V., 2000. Basic geological features of the Dinarides and South Tisia. In: J. Pamić, B. Tomljenović (Eds.), *Pancardi 2000 Fieldtrip Guidebook*. *Vijesti*, 37: 9-18.
- Pamić J., 2002. The Sava-Vardar Zone of the Dinarides and Hellenides versus the Vardar Ocean. *Ecl. Geol. Helv.*, 95: 99-113.
- Pamić J., Tomljenović B. and Balen D., 2002. Geodynamic and petrogenetic evolution of Alpine ophiolites from the central and NW Dinarides: an overview. *Lithos*, 65: 113-142.
- Parkinson C., 1998. Emplacement of the East Sulawesi Ophiolite: evidence from subophiolite metamorphic rocks. *J. Asian Earth Sci.*, 16: 13-28.
- Pearce J.A. and Peate D.W., 1995. Tectonic implications of the composition of volcanic arc magmas. *Ann. Rev. Earth Planet. Sci.*, 23: 251-285.
- Peacock S.M., Rushmer T. and Thompson A.B., 1994. Partial melting of subducting oceanic crust. *Earth Planet. Sci.*, 121: 227-244.
- Pinter N., Gyula G., Weber J., Stein S. and Medak D. (Eds.), 2006. *The Adria Microplate: GPS Geodesy, Tectonics and Hazards*. Nato Science Series. IV: Earth and Environmental Sciences. Kluwer Acad. Publ., Dordrecht.
- Pouchou J.L. and Pichoir F., 1984. A new model for quantitative analyses. I. Application to the analysis of homogeneous samples. *Rech. Aerospat.*, 3: 13-38.
- Pouchou J.L. and Pichoir F., 1985. "PAP" (ϕ - ρ -Z) correction procedure for improved quantitative microanalysis. In: J.T. Armstrong (Ed.), *Microbeam analysis*. Press Intern. San Francisco, p. 104-106.
- Prakash D., Arima M. and Mohan A., 2007. Ultrahigh-temperature mafic granulites from Panrimalai, south India: Constraints from phase equilibria and thermobarometry. *J. Asian Earth Sci.*, 29: 41-61.
- Raase P., Raith M., Ackermann D. and Lal R.K., 1986. Progressive metamorphism of mafic rocks from greenschist to granulite facies in the Dharwar Craton of South India. *J. Geol.*, 94: 261-282.
- Rathossi C. and Pontikes Y., 2010. Effect of firing temperature and atmosphere on ceramics made of NW Peloponnese clay sediments: Part II. Chemistry of pyrometamorphic minerals and comparison with ancient ceramics. *J. Eur. Ceram. Soc.*, 30: 1853-1866.
- Robertson A., 2004. Development of concepts concerning the genesis and emplacement of Tethyan ophiolites in the Eastern Mediterranean and Oman regions. *Earth Sci. Rev.*, 66: 331-387.

- Rollinson H., 1993. Using geochemical data evaluation, presentation, interpretation. Longman, Essex, 352 pp.
- Romano S.S., Brix M.R., Dörr W., Fiala J., Krenn E. and Zulauf G., 2006. The Carboniferous to Jurassic evolution of the pre-Alpine basement of Crete: constraints from U-Pb and U-Th-Pb dating of orthogneiss, fission-track dating of zircon, structural and petrological data. In: A.H.F. Robertson and D. Mountrakis (Eds.), Tectonic development of the Eastern Mediterranean region, *Geol. Soc. London Spec. Publ.*, 260: 34-52.
- Ruiz Cruz M.D., 2003. Two stages of "metamorphic vermiculite" growth in schists from the Maláguide Complex, Betic Cordillera, Spain. *Can. Mineral.*, 41: 1397-1412.
- Saccani E., Beccaluva L., Photiades A. and Zeda O., 2011. Petrogenesis and tectono-magmatic significance of basalts and mantle peridotites from the Albanian-Greek ophiolites and sub-ophiolitic mélanges. New constraints for the Triassic-Jurassic evolution of the Neo-Tethys in the Dinaride sector. *Lithos*, 124: 227-242.
- Saunders A.D. and Tarney J., 1979. The geochemistry of basalts from a back-arc spreading centre in the East Scotia Sea. *Geochim. Cosmochim. Acta*, 43: 555-572.
- Schiffman P. and Day H.W., 1999. Petrological methods for the study of very low grade metabasites. In: M. Frey and D. Robinson (Eds.), *Very Low Grade metamorphism*. Blackwell Scientific, Oxford, p. 108-142.
- Schmid S.M., Bernoulli D., Fügenschuh B., Matenco L., Schefer S., Schuster R., Tischler M. and Ustaszewski K., 2008. The Alpine-Carpathian-Dinaridic orogenic system: correlation and evolution of tectonic units. *Swiss J. Geosci.*, 101: 139-183.
- Schmidt M.W., 1992. Amphibole composition in tonalite as a function of pressure: an experimental calibration of the Al-in-hornblende barometer. *Contrib. Mineral. Petrol.*, 110: 304-310.
- Shervais J.W., 1982. Ti-V plots and the petrogenesis of modern and ophiolitic lavas. *Earth Planet. Sci. Lett.*, 59: 101-118.
- Šegvić B., Lugović B. and Ignjatić S., 2005. Petrochemical and geotectonic characteristics of amphibolites from the Zagorje-Mid-Transdanubian shear Zone (Kalnik Mt., Croatia). In: I. Velić, I. Vlahović and R. Biondić (Eds.), *Abstract Book, 3rd Croatian Geol. Congr., Opatija, Croatia*, p. 143-144.
- Šegvić B., Šešelj L., Slovenec D., Lugović B. and Ferreira Mählmann R., 2012. Composition, technology of manufacture, and circulation of Hellenistic pottery from the Eastern Adriatic: A case study of three archaeological sites along the Dalmatian coast, Croatia. *Geoarchaeology*, 27: 63-87.
- Slovenec Da. and Pamić J., 2002. Geology of Vardar Zone ophiolites of the Medvednica Mountain area located along the Zagreb-Zemlin Line (NW Croatia). *Geol. Carpath.*, 53: 53-59.
- Slovenec Da. and Lugović B., 2008. Amphibole gabbroic rocks from the Mt. Medvednica ophiolite mélange (NW Croatia): geochemistry and tectonic setting. *Geol. Carpath.*, 59: 277-293.
- Slovenec Da. and Lugović B., 2009. Geochemistry and tectono-magmatic affinity of extrusive and dyke rocks from the ophiolite mélange in the SW Zagorje-Mid-Transdanubian Zone (Mt. Medvednica, Croatia). *Ophioliti*, 34: 63-80.
- Slovenec Da., Lugović B. and Vlahović I., 2010. Geochemistry, petrology and tectonomagmatic significance of basaltic rocks from the ophiolite mélange at the NW External-Internal Dinarides junction (Croatia). *Geol. Carpath.*, 61: 273-292.
- Slovenec Da., Lugović B., Meyer H.-P. and Šiftar Garapić G., 2011. A tectono-magmatic correlation of basaltic rocks from ophiolite mélanges at the north-eastern tip of the Sava-Vardar suture Zone, Northern Croatia, constrained by geochemistry and petrology. *Ophioliti*, 36: 77-100.
- Slovenec Da. and Lugović B., 2012. Evidence of the spreading culmination in the Eastern Tethyan Repno oceanic domain, assessed by the petrology and geochemistry of N-MORB extrusive rocks from the Mt. Medvednica ophiolite mélange (NW Croatia). *Geol. Croat.*, 65: 435-446.
- Stampfli G. M., Borel G.D., Marchant R. and Mosar J., 2002. Western Alps geological constraints on western Tethyan reconstructions. In: G. Rosenbaum and G.S. Lister (Eds.), *Reconstruction of the evolution of the Alpine-Himalayan Orogen*. *J. Virtual Explorer*, 7: 75-104.
- Sun S.S. and McDonough W.F., 1989. Chemical and isotopic systematics of oceanic basalts: implications for mantle composition and processes. In: A.D. Saunders and M.J. Norry (Eds.), *Magma-tism in ocean basins*. *Geol. Soc. London Spec. Publ.*, 42: 313-345.
- Šimunić A., Pikija M., Hećimović I. and Šimunić A., 1981. Osnovna geološka karta SFRJ 1:100000. Tumač za list Varaždin. *Inst. Geol. Istraž. Zagreb, Savezni Geol. Zavod Beograd*, p. 1-81.
- Šimunić A., Pikija M. and Hećimović I., 1982. Osnovna geološka karta SFRJ 1:100000, list Varaždin. *Inst. Geol. Istraž. Zagreb, Savezni Geol. Zavod Beograd*.
- Tomljenović B., Csontos L., Márton E. and Márton P., 2008. Tectonic evolution of the northwestern Internal Dinarides as constrained by structures and rotation of Medvednica Mountains, North Croatia. *Geol. Soc. London Spec. Publ.*, 298: 145-167.
- Ustaszewski K., Schmid S.M., Lugović B., Schuster R., Schaltegger U., Bernoulli D., Hottinger L., Kounov A., Fügenschuh B. and Schefer S., 2009. Late Cretaceous intra-oceanic magmatism in the internal Dinarides (northern Bosnia and Herzegovina): Implications for the collision of the Adriatic and European plates. *Lithos*, 108: 106-125.
- Vernon R.H. and Clarke G.I., 2008. *Principles of metamorphic petrology*. Univ. Press, Cambridge, 446 pp.
- Vrkljan M. and Garašić V., 2004. Different geochemical signatures developed in some basic magmatic rocks of Mt. Kalnik (North Croatia). *R-G-N Zbornik*, 16: 65-73.
- Wakabayashi J. and Dilek Y., 2000. Spatial and temporal relationships between ophiolites and their metamorphic soles: a test of model of forearc ophiolite genesis. In: Y. Dilek, E.M. Moore, D. Elthon and A. Nicolas (Eds.), *Ophiolites and oceanic crust: New insights from field studies and the ocean drilling program*. *Geol. Soc. Am. S.*, 349: 53-64.
- Weaver S.D., Saunders A.D., Pankhurst R.J. and Tarney J., 1979. A geochemical study of magmatism associated with the initial stages of back-arc spreading. *Contrib. Mineral. Petrol.*, 68: 151-169.
- Winchester J.A. and Floyd P.A., 1977. Geochemical discrimination of different magma series and their differentiation products using immobile elements. *Chem. Geol.*, 20: 325-343.
- Wolf M.B. and Wyllie P.J., 1993. Garnet growth during amphibolite anatexis: implications of a garnetiferous restite. *J. Geol.*, 101: 353-373.
- Wolf M.B. and Wyllie P.J. 1994. Dehydration-melting of amphibolite at 10 kbar: the effects of temperature and time. *Contrib. Mineral. Petrol.*, 115: 369-383.
- Wood D.A., 1980. The application of a Th-Hf-Ta diagram to problems of tectonomagmatic classification and to establishing the nature of crustal contamination of basaltic lavas of the British Tertiary Volcanic Province. *Earth Planet. Sci. Lett.*, 50: 11-30.
- Wood B.J. and Banno S., 1973. Garnet-orthopyroxene and orthopyroxene-clinopyroxene relationships in simple and complex systems. *Contrib. Mineral. Petrol.*, 42: 109-124.
- Woodsworth G.J., 1977. Homogenization of zoned garnets from pelitic schists. *Can. Mineral.*, 15: 230-242.